A cross-species proteomic map of synapse development reveals neoteny during human postsynaptic density maturation

Authors: Li Wang[1,2]*, Kaifang Pang[3,4], Li Zhou[1,2], Arantxa Cebrián-Silla[1,5], Susana González-Granero[6], Shaohui Wang[1,2], Qiuli Bi[1,2], Matthew L. White[1,2], Brandon Ho[1,2], Jiani Li[7], Tao Li[1], Yonatan Perez[1,2], Eric J. Huang[8], Ethan A. Winkler[5], Mercedes F. Paredes[1,2], Rothem Kovner[9], Nenad Sestan[9], Alex A. Pollen[1,2], Pengyuan Liu[10], Jingjing Li[1,2], Xianhua Piao[1,11,12], José Manuel García-Verdugo[6], Arturo Alvarez-Buylla[1,5], Zhandong Liu[3,4], Arnold R. Kriegstein[1,2]*

Affiliations:

[1]The Eli and Edythe Broad Center of Regeneration Medicine and Stem Cell Research, University of California San Francisco; San Francisco, CA 94143, USA.

[2]Department of Neurology, University of California San Francisco; San Francisco, CA 94143, USA.

[3]Jan and Dan Duncan Neurological Research Institute at Texas Children's Hospital; Houston, Texas 77030, USA.

[4]Department of Pediatrics, Baylor College of Medicine; Houston, Texas 77030, USA.

[5]Department of Neurological Surgery, University of California San Francisco; San Francisco, CA 94143, USA.

[6]Laboratory of Comparative Neurobiology, Cavanilles Institute of Biodiversity and Evolutionary Biology, University of Valencia and CIBERNED; Valencia, Spain.

[7]Gilead Sciences, Foster City, CA 94404, USA.

[8]Department of Pathology, University of California San Francisco; San Francisco, CA 94143, USA.

[9]Department of Neuroscience, Yale School of Medicine, New Haven, CT 06520, USA

[10]Department of Chemistry, University of Massachusetts Lowell; Lowell, MA 01854, USA.

[11]Division of Neonatology, Department of Pediatrics, University of California San Francisco; San Francisco, CA 94158, USA.

[12]Newborn Brain Research Institute, University of California San Francisco; San Francisco, CA 94158, USA.

*Corresponding author. Email: Li.Wang@ucsf.edu or Arnold.Kriegstein@ucsf.edu.

Abstract: The molecular mechanisms and evolutionary changes accompanying synapse development are still poorly understood. Here, we generated a cross-species proteomic map of synapse development in the human, macaque, and mouse neocortex. By tracking the changes of >1,000 postsynaptic density (PSD) proteins from midgestation to adolescence, we found that PSD maturation in humans separates into three major phases that are dominated by distinct pathways. Cross-species comparisons reveal that the human PSD matures about three times slower than other species and contains higher levels of Rho guanine nucleotide exchange factors (RhoGEFs) in the perinatal period. Enhancement of the RhoGEF signaling in human neurons delays the morphological maturation of dendritic spines and functional maturation of synapses, potentially contributing to the neotenic traits of human brain development. In addition, PSD proteins can be

divided into four modules that exert stage- and cell type-specific functions, possibly explaining their differential associations with cognitive functions and diseases. Together, our proteomic map of synapse development provides a blueprint for studying the molecular basis and evolutionary changes of synapse maturation.

Main Text:

Synapses establish the neuronal networks that mediate information processing in the brain. Synaptic dysfunction plays a critical role in most, if not all, brain diseases, including disorders that typically occur in childhood, adolescence, or adulthood (*1–3*). Therefore, understanding the formation, maturation, and specification of synapses is essential for understanding human cognition and mental disorders.

The postsynaptic density (PSD) is a highly specialized structure located beneath the postsynaptic membrane of excitatory synapses. Biochemical isolation of PSDs from the adult brain followed by mass spectrometry revealed that the PSD is a highly sophisticated protein complex composed of >1,000 proteins including cytoskeletal proteins, neurotransmitter receptors, signaling enzymes, ribosomal proteins, and scaffolding proteins (*4*). Mutations in these proteins cause over 130 brain diseases (*5*).

Excitatory synapses and associated PSDs undergo profound changes at both morphological and compositional levels during brain development (*6–10*). In particular, developmental increases in the ratio of N-methyl-D-aspartic acid (NMDA) receptor subunits GRIN2B to GRIN2A and of PSD scaffolding proteins DLG3 to DLG4 are critical for the functional maturation of synapses (*11–13*). However, studies to understand the developmental changes of the PSD are limited to dozens of well-known PSD proteins typically identified in the adult brain (*6*, *8*, *9*). Unbiased, systematic characterization has been lacking. In addition, density, composition, and maturation rates of synapses differ between species, potentially contributing to the evolutionary variation of neurotransmission properties, cognitive ability, and behavioral repertoire (*14–20*). For example, prolonged maturation or neoteny of human synapses has been suggested as a possible explanation for the emergence of human-specific cognitive traits (*21–23*). But we still know little about the underlying molecular mechanisms.

Here, we generate a cross-species proteomic map of synapse development in the neocortex, identifying the dynamics of >1,000 PSD proteins and the molecular pathways that govern individual phases of synapse maturation. A comparison of the maturing PSDs in humans to those in macaques and mice reveals that PSD maturation in humans is approximately three times slower than that in other species. Moreover, Rho guanine nucleotide exchange factors (RhoGEFs), which serve to delay synapse maturation, are more abundant in human PSDs in the perinatal phase, possibly contributing to the neotenic traits of human synapses. Integrating these data with transcriptomic and genetic data, we further determine the gene regulatory network, cell type specificity, and selective disease vulnerability of synapse maturation. Our data provide a temporal map of the topology of synapse development in the neocortex and offer insight into the evolutionary mechanisms of synaptic neoteny in humans.

Results

Changes in PSD composition during human neocortical development

To understand the molecular changes of the PSD in the developing human neocortex, we obtained neocortical samples across six major developmental stages ranging from the second trimester to

adolescence (Fig. 1A and table S1). The six stages were chosen to cover major developmental events including neurogenesis, neuronal migration, synaptogenesis, myelination, and synaptic pruning. PSDs were isolated from each sample as described previously (*24*). Isolation of the PSD, including from immature human brain samples, was successful as indicated by the following quality control metrics. Integral components of the PSD, but not presynaptic (SYP) or cytoplasmic (GAPDH) proteins, were enriched in the PSD fraction of early-stage samples (fig. S1A). In addition, electron microscopy identified typical PSD-like electron-dense structures in the PSD fraction of immature samples (fig. S1B). Furthermore, GRIN2B and DLG4, two PSD proteins that decrease and increase, respectively, during PSD maturation (*8*), showed the expected abundance patterns in isolated PSDs (fig. S1C). Finally, the yield of PSDs correlated well with the estimated number of synapses (fig. S1D).

We performed liquid chromatography and tandem mass spectrometry (LC-MS/MS) analysis and label-free quantification on 54 PSD samples. Each PSD sample was isolated from a different neurologically normal individual and had passed screening for synaptic proteome preservation (*25*). The identified proteins overlapped significantly with previously reported PSD proteins at comparable stages (fig. S1E) (*5*, *26*). After the removal of potential contaminants, we found a total of 1765 PSD proteins in at least one of the six developmental stages (fig. S1F and table S2). To assess the quality of the data, we first sought to determine whether developmental changes were the main driver of variance. Principal component (PC) analysis revealed that samples from the same age group were closely clustered (Fig. 1B). PC1, accounting for 39.5% of the variability, was strongly correlated with the age of the samples, but not with other potential confounding factors like sex or processing batch (fig. S1G). Moreover, variance across age groups explains a median of 41.7% of the variation in the dataset, after correcting for processing batch, PSD quality, and sex (fig. S1G). Hierarchical clustering also showed that samples were clustered by age (Fig. 1C). Proteins such as GRIN2A, GRIN2B, DLG3, and DLG4 showed the expected abundance patterns during PSD maturation and were consistent with Western blotting data (Fig. 1C and fig. S2, A and B). To validate the identified PSD proteins *in situ* in the immature human neocortex, we performed immunostaining of several proteins that show enrichment at midgestation, including the ribosomal subunit RPS6, β-catenin (CTNNB1), the vesicle trafficking regulator GDI1, and the actin modulator cofilin (CFL1). All these proteins colocalized with the canonical PSD marker DLG4 in a subset of synapses (fig. S3, A to D).

We performed gene set enrichment analysis (GSEA) to identify molecular pathways with higher activity at individual developmental stages compared with other stages. In general, PSD maturation appears to undergo three major phases (midgestational, perinatal, and postnatal). The midgestational phase, between gestational week 18 to 23, was enriched for translation-related pathways (Fig. 1, D and E, and fig. S2C). The perinatal phase, between the third trimester and one year of age, was enriched for Rho GTPase and protein folding pathways (Fig. 1, D and E, and fig. S2D). The postnatal phase, above four years of age, was enriched for synaptic transmission-related pathways (Fig. 1, D and E, and fig. S2E). These results suggest that local protein synthesis, actin cytoskeleton reorganization, and enhancement of synaptic efficacy were sequentially activated during PSD development. At the individual protein level, proteins from the same complex or pathway generally tend to exhibit similar abundance changes during development (Fig. 1E and fig. S2, C to E). However, relative changes in the abundance of homologous proteins such as GRIN2A/GRIN2B and DLG3/DLG4, as shown above, are critical for synapse maturation (*11–13*). Another example is the two predominant α-amino-3-hydroxy-5-methyl-4-isoxazolepropionic acid (AMPA) receptor subunits GRIA1 and GRIA2. We found that GRIA2 increased steadily during

development, whereas GRIA1 remained relatively constant (Fig. 1E), consistent with GRIA2-lacking, and thus calcium-permeable AMPA receptors being important for early synaptic function (*27*). In addition to these proteins, we discovered many other homologous proteins that exhibited reciprocal pattern changes (Fig. 1F and fig. S4, A to H) including drebrin/drebrin-like proteins, whose abundance changes were further validated by immunostaining (Fig. 1G and fig. S5, A to D). These newly identified reciprocal changes may also play important roles in PSD maturation.

Protein modules and their coordinated functions in the PSD

Proteins with similar abundance patterns during PSD maturation could represent protein modules with specific molecular functions. We identified four protein modules based on correlation by weighted correlation network analysis (WGCNA) (Fig. 2A) (*28*). All four modules were significantly enriched for protein-protein interactions (PPIs), whereas no enrichment was found for proteins with no module assignment (the grey module) (Fig. 2B), suggesting that proteins in the same module work synergistically by forming protein complexes. Indeed, pathway overrepresentation analysis highlighted module-specific enrichment in particular biological pathways (Fig. 2C and table S3). Proteins in the brown module had higher abundance in the second trimester and became lowly abundant in the third trimester and thereafter (Fig. 2A). The brown module was enriched with translation-related pathways, highlighting the role of local protein synthesis in the midgestational phase of PSD development (Fig. 2C). The blue module also showed high abundance in the second trimester. However, its level decreased more slowly compared with the brown module and remained relatively high in the third trimester (Fig. 2A). The blue module was enriched for signaling pathways related to axon guidance and Rho GTPases, highlighting the roles of synapse specification and actin remodeling in both the midgestational and perinatal phases of PSD maturation (Fig. 2C). The other two modules, turquoise and yellow, both peaked postnatally, with the turquoise module peaking earlier shortly after birth (Fig. 2A). Rho GTPase signaling was preferentially active in the turquoise module, indicating, again, a selective role of actin remodeling in the perinatal phase of PSD maturation (Fig. 2C). Synaptic transmission pathways were enriched in both modules, suggesting that the main theme of PSD maturation in the postnatal phase is to make synapses more robust and efficient (Fig. 2C). Similar results were obtained by synaptic gene ontology (SynGO) enrichment analysis (fig. S6A and table S3) (*29*). In summary, abundance patterns and molecular functions of the PSD protein modules are consistent with the GSEA results at individual developmental stages.

To visualize potential protein complexes and interactions in the PSD, we generated PPI-co-abundance networks in each module (see Materials and Methods) (figs. S6B, S7, and S8). As expected, proteins involved in the same pathway were clustered more closely, as indicated by a shorter average path length to each other than to proteins outside the pathway (fig. S6, B and C). PPIs and biological functions of a protein are often mediated by protein domains. We determined the distribution of protein domains in the modules (Fig. 2D) and the domain architecture of individual proteins (fig. S9 and table S4). Domains involved in vesicle trafficking (RAB and t_SNARE), cell adhesion (LRR, CA, and ARM), signal transduction (S_TKc, C1, and C2), and adult PSD scaffolds (PDZ, SH3, and GuKc) (*9*) were enriched in the brown, blue, turquoise, and yellow modules, respectively (Fig. 2D). Interestingly, although both the blue and turquoise modules were involved in Rho GTPase signaling (Fig. 2B), RhoGAP and RhoGEF domains were selectively enriched in each of them (Fig. 2D). Indeed, Rho GTPase-activating proteins (RhoGAPs), particularly those specific for Rac1 and Cdc42, were enriched in the blue module (Fig.

2, E and F, and table S4). Instead, Rho guanine nucleotide exchange factors (RhoGEFs), particularly those specific for Rac1, were enriched in the turquoise module (Fig. 2, E and F). Given the critical role of Rho GTPases in actin remodeling, these results suggest that Rho GTPase signaling is dynamically regulated during PSD maturation to facilitate stage-specific cytoskeleton reorganization requirements and morphological changes.

Transcription of PSD proteins and its cell type specificity

To understand the role of transcription in regulating PSD development, we compared the RNA levels of PSD modules with their abundance patterns. Integrating the BrainSpan and PsychENCODE transcriptomic data (*30*, *31*) from the developing human neocortex with our proteomic data, we found that the general trends were preserved while the differences between the brown and blue modules and between the turquoise and yellow modules were largely diminished (Fig. 3A). For example, Rho GTPase regulators and PSD scaffolding proteins from the turquoise and yellow modules, respectively, had distinct abundance patterns in the proteomic data, but they had similar expression patterns in the transcriptomic data (Fig. 3B). To quantify the concordance between RNA and protein, we calculated the Spearman's rank coefficient of correlation between RNA and protein levels of all PSD proteins (table S5). We found that proteins in the blue and yellow modules generally had high RNA-protein concordance (median Spearman $r > 0.5$) (Fig. 3C). In contrast, brown and turquoise modules had significantly lower concordance (Fig. 3C), suggesting that post-transcriptional regulatory mechanisms such as protein transport play a key role in recruiting proteins to the PSD in these two modules. Consistent with these results, module density and connectivity preservation analysis (*32*) showed that although all four modules were at least moderately preserved in the transcriptomic data, the brown and turquoises module were among the least preserved (fig. S10A).

Given their high RNA-protein concordance, we next focused on the blue and yellow modules to study the regulatory mechanisms of their transcription. Transcription factor (TF) enrichment analysis by ChEA3 revealed core TF networks targeting the two modules (Fig. 3D and table S5). Some TFs in the networks such as FOXG1, MEIS2, MYT1L, and RORB are known to be critical regulators of neuronal differentiation and synapse development.

To examine transcription of the blue and yellow modules in a cell type-specific manner, we integrated our PSD proteomic data with single-cell RNA-sequencing data from both the developing and adult human neocortex (*33*, *34*) (fig. S10, B to D). In the developing neocortex, expression of genes in the blue module showed variation between neuronal subtypes but remain relatively constant over time in the second trimester (Fig. 3E). In contrast, expression of genes in the yellow module displayed distinct patterns in different neuronal subtypes (Fig. 3E). The yellow module positively correlated with the temporal maturity of the PSD (Fig. 2A). Consistent with the fact that synapses just start to form as neurons are migrating, yellow module genes remained lowly expressed in immature excitatory neurons. For more mature glutamatergic neurons, the expression levels were dependent on both sample age and neuronal birth order. Specifically, levels were higher in (1) older samples and (2) earlier-born deep-layer neurons than later-born upper-layer neurons (Fig. 3E). Interestingly, Cajal Retzius cells, which are the first glutamatergic neurons to emerge in the neocortex, showed little change in yellow module levels, consistent with their transient role in cortical organization rather than in synaptic circuit formation (Fig. 3E). Another subclass of neurons, GABAergic interneurons, are generated in a similar time window as glutamatergic neurons in the neocortex. However, their yellow module levels were lower than those of most glutamatergic neuron subtypes (Fig. 3E), reflecting their long-range migration and

late integration into the neocortex. Together, these results indicate that transcription of PSD proteins is stage- and cell type-specific and is tightly controlled to regulate synapse formation and maturation.

Although PSDs in GABAergic interneurons appeared to mature slower than those in glutamatergic neurons during early development, they might reach a similar level of maturity later. Surprisingly, we found that GABAergic interneurons had higher levels of genes in the blue module and lower levels of genes in the yellow module in the adult neocortex (Fig. 3F and fig. S11A). Thus, compared with glutamatergic neurons, interneurons maintain higher expression of genes encoding early-stage synaptic proteins at fully mature stages. This could be attributed to the differential expression of TFs targeting the two modules (Fig. 3G and fig. S11B). Differences in transcription and abundance of PSD proteins may contribute to the differential excitatory postsynaptic responses observed in these two subclasses of cortical neurons (*35*).

Species differences in PSD development

Excitatory synapses and the PSD in humans, macaques, and mice are similar yet they differ at both the morphological and molecular levels (*17*, *19*, *36*). However, the changes in PSD development that contribute to these differences are not known. Therefore, we profiled macaque and mouse neocortical PSDs using the same method at five time points (Fig 4A and table S7). These time points roughly correspond to the developmental stages of our human samples (*37*). We identified a total of 1572 proteins in both developing macaque and mouse PSDs (table S8 and S9). Most of the identified proteins were found in multiple age groups, whereas some were stage-specific (fig. S12, A and B). Both PC analysis and hierarchical clustering showed that samples clustered by age group, confirming that developmental changes and not technical noise contributed to the variance in the data (fig. S12, C to F). GSEA showed that, as in humans, translation-related pathways and synaptic transmission-related pathways were more active in the early and late PSD development, respectively, in both macaques and mice (Fig. 4B). However, enrichment of Rho GTPase signaling and the Rac1 pathway found in the perinatal phase of PSD development in humans was largely diminished in macaques and mice (Fig. 4B).

To quantitatively compare PSD samples from different species, we performed cross-species similarity analysis. We calculated the Pearson correlation coefficients between PSD samples from different species and found that human samples in the second trimester and above four years of age correlated well with macaque and mouse samples at corresponding stages (Pearson $r > 0.6$) (Fig. 4C and table S10). However, human samples between the third trimester and one year of age (the perinatal phase) showed relatively low correlations with all age groups in other species. We then sought to identify changes in PSD proteins that led to this difference.

Different species have distinct developmental timescales, making it hard to directly compare the abundance of PSD proteins. We therefore applied a regularized linear approach (see Materials and Methods) to unbiasedly predict the equivalent PSD ages of all three species based on their proteomic profiles (Fig. 4D and table S10). We found that multiplicative changes in real age were approximately linearly associated with multiplicative changes in the predicted equivalent human PSD age, except that macaque samples appeared to undergo two different stages separated by one year of age (Fig. 4D). We thus regressed the log-transformed humanized ages against the real log-transformed ages using a linear model (or a linear spline model for macaque samples) and obtained the slope coefficients as an estimator of PSD maturation rate normalized to the developmental

timescale of individual species. This analysis revealed that PSD maturation was about three times slower in humans than in mice and macaques (< 1 year) (Fig. 4D).

Based on the equivalent PSD ages, we compared the abundance patterns of the human PSD modules in all three species. While the patterns of the blue and yellow modules were similar across all species, the brown and turquoise modules displayed species-specific differences (Fig. 4E). Specifically, the brown module was less abundant, and the turquoise module was more abundant in humans at the perinatal phase, likely causing the low correlation we observed in the similarity analysis at this developmental stage. Accordingly, module density and connectivity preservation analysis showed that the brown and turquoise modules were among the least preserved in macaques and mice (fig. S12, G and H). In conclusion, human PSD matures at a slower rate and the perinatal phase of its development is less represented in macaques and mice.

Enhancement of RhoGEF signaling promotes neoteny of human synapses

The slower maturation rate of the human PSD could result from the increased abundance of turquoise module proteins and enrichment of Rho GTPase regulators at the perinatal phase. To test this hypothesis, we further investigated the increase of RhoGEF signaling in the human PSD. Indeed, all RhoGEF proteins in the turquoise module were drastically increased at the perinatal phase in humans and remained more abundant than in other species thereafter in our proteomic data (Fig. 5A). This finding was further confirmed by Western blotting (Fig. 5B and fig. S13A) and immunostaining (Fig. 5C and fig. S14). Postmortem accumulation could lead to an artificial increase in PSD proteins as has been reported for tubulins (*38*). To rule out the possibility that postmortem accumulation caused the observed increase in RhoGEF proteins, we compared PSDs prepared from postmortem samples (postmortem interval between 14 to 17 hours) with those from neurosurgical biopsy and found that RhoGEF levels were comparable (fig. S13B). Next, we tested whether the increase in RhoGEF proteins led to the activation of their known downstream pathways. A majority of RhoGEF proteins in the turquoise module target Rac1 for Rho GTPase activation. We found that phosphorylation of PAK, an indicator of Rac1 activity, increased in human synaptosomes along with RhoGEFs during synapse maturation (Fig. 5D). However, no change was observed in mouse neurons (Fig. 5D). Taken together, these results validated the enhancement of RhoGEF signaling in the human PSD.

To understand the role of RhoGEF proteins in human synapse maturation, we individually overexpressed two RhoGEF proteins in the turquoise module, ARHGEF7 and RASGRF2, in developing human cortical neurons (fig. S15). The density of synapses, quantified by DLG4 and SYN1 co-staining, was similar (Fig. 5E), indicating that synaptogenesis was not affected. However, analysis of the morphology of dendritic spines revealed that overexpressing either ARHGEF7 or RASGRF2 increased spine length and promoted the formation of immature-looking, filopodia-like spines (Fig. 5E). We also observed a significant increase in spine density in RhoGEF overexpressing neurons (Fig. 5E). To test whether these morphological changes translate into functional consequences, we recorded miniature excitatory postsynaptic currents (mEPSCs) in human neurons with and without RhoGEF overexpression. We found that mEPSC frequency was significantly decreased in neurons overexpressing either ARHGEF7 or RASGRF2 (Fig. 5F). Moreover, the surface level of AMPA receptor GRIA1 was reduced by ARHGEF7 or RASGRF2 overexpression (Fig. 5G and fig. S16). These data demonstrate that overexpression of specific RhoGEF proteins inhibits the functional maturation of synapses. Altogether, our results suggest that the human-specific increase in selective RhoGEF proteins delays maturation and promotes neoteny of human synapses.

PSD modules in human cognition and brain disorders

We next investigated whether genetic variants associated with human cognition converge onto the human PSD modules, identifying that the turquoise module was enriched for GWAS signals of processing speed and fluid intelligence (the UK Biobank) (Fig. 6A). The turquoise module has its peak expression shortly after birth, at which time infants perceive a wealth of external stimuli. Thus, we posited that proteins in this module were important for activity-dependent synaptic remodeling. Indeed, the turquoise module was highly enriched for activity-dependent proteins in neurons (Odds ratio > 3; Fig. 5B and table S11) (*39*), including TRIM3 (an activity-dependent ubiquitin ligase for PSD scaffolding proteins) (*40*), GRIPAP1 (a recycling endosome regulator critical for synaptic plasticity) (*41*), and RhoGEF proteins such as ABR and NGEF (fig. S17A). Combined with the fact that the turquoise module is more abundant in the human PSD and that RhoGEF proteins in this module promote synaptic neoteny, these results highlight the possible significance of this module in the evolutionary enhancement of human cognitive function.

Synaptic dysfunction contributes to both neurodevelopmental and psychiatric disorders, often caused by *de novo* and common variants, respectively. Regarding *de novo* variants, genes encoding PSD proteins were more intolerant of protein-truncating variants (PTVs) (lower LOEUF scores) and missense variants (higher missense Z-scores) compared with all genes expressed in the neocortex (Fig. 6C), suggesting that mutations in these genes are more likely to cause human diseases. Remarkably, the turquoise module was particularly intolerant of missense variants (Fig. 6C). No difference was observed for synonymous mutations (fig. S17B). Accordingly, we found that genes encoding PSD proteins were enriched for *de novo* nonsynonymous variants associated with neurodevelopmental disorders including epilepsy, developmental delay (DD), and intellectual disability (ID) (denovo-db) (Fig. 6D, fig. S17, C and D, and table S11). In particular, the turquoise module had an excessive number of missense variants, whereas the yellow module was enriched for both missense variants and PTVs. Turquoise module genes with disease-associated missense variants included genes encoding ion channels such as *KCNQ2* and *SCN2A* and molecular motors such as *DYNC1H1* and *KIF1A*. Some of these missense variants may be gain-of-function or dominant-negative mutations that have different pathogenic effects compared with PTVs (*42*, *43*). In contrast, many yellow module genes with PTVs were genes encoding enzymes that regulate PSD organization and postsynaptic receptor trafficking, such as *SYNGAP1*, *IQSEC2*, and *CDKL5*. Therefore, although mutations in both modules contribute to neurodevelopmental disorders, the different patterns of module abundance and variant type enrichment suggest that they do so by different mechanisms that target distinct stages of synapse maturation.

For psychiatric disorders, the brown module was enriched for GWAS signals of diseases that generally manifest in young adulthood, including schizophrenia (SCZ), bipolar disorder (BPD), and major depressive disorder (MDD) (The Psychiatric Genomics Consortium) (Fig. 6E, fig. S18A, and table S11). Proteins in the brown module had peak abundance at midgestation, indicating an early etiology involving synapse development for these adolescence/adult-onset disorders. However, after the onset of these psychiatric disorders, genes encoding PSD proteins in the late modules (turquoise and yellow) were downregulated compared with controls (Fig. 6F, fig. S18, B and C, and table S11). This is likely the consequence of a downstream cascade of biological events following earlier-acting genetic risk factors that disrupt synapse development.

Discussion

Although synapses and the PSD are known to undergo profound remodeling in brain development to enable the formation and reorganization of brain networks (*6*, *8*, *44*), we have had limited knowledge of the molecular changes that occur during this remodeling. In this study, we generated a cross-species proteomic map of synapse development and revealed the temporal dynamics of >1,000 PSD proteins. We demonstrate that the human PSD undergoes three major phases of maturation. By relating the abundance of PSD proteins to each other, we further uncovered individual protein modules and networks that exert stage-, cell type-, and species-specific functions. Furthermore, we found that the PSD develops about three times slower in humans than in other species and that the increased abundance of RhoGEF proteins, as expressed in the turquoise module, contributes to this difference. The turquoise module is also associated with synaptic plasticity, human cognitive function, and mental disorders. Together, these data provide a blueprint for studying the molecular and evolutionary mechanisms of synapse maturation in humans.

Synapse development is regulated at both the RNA and protein levels (*45*). By integrating PSD proteomic data with bulk RNA-sequencing data, we found that different PSD modules exhibit different RNA-protein concordance, suggesting that they are differentially regulated by post-transcriptional mechanisms. Focusing on the modules with high RNA-protein concordance, we inferred neuronal subtype-specific PSD signatures from single-cell RNA-sequencing data. Our analysis revealed major differences in the PSD between glutamatergic and GABAergic neuronal subtypes in both the developing and adult neocortex. This is consistent with previous studies showing that the composition of the PSD is diverse among neuronal subtypes (*46–48*). One limitation of this inference is that single-cell RNA-sequencing does not include RNAs in dendrites that could contribute to the PSD through local translation. Although somatic and dendritic RNAs are significantly correlated (*49*), future studies to determine the proteomic profiles of neuronal subtype-specific PSDs will help expand these findings.

Previous studies identified a critical role of a RhoGAP protein, SRGAP2, in the human-specific developmental delay in synapse maturation and increase in synaptic density (*50–52*). It has been shown that the Rac1-GAP activity of the ancestral protein SRGAP2A limits the spine neck length and density in neocortical neurons. Human-specific partial duplications of SRGAP2 inhibited the function of SRGAP2A, resulting in longer spine necks and higher spine density in humans. In our study, we found that multiple RhoGEF proteins targeting Rac1 have increased abundance in the human PSD starting at the perinatal stages. Enhancement of RhoGEF signaling in human neurons not only increased spine length and density but also delays functional maturation of synapses. Given that RhoGAP and RhoGEF proteins exert antagonistic functions in activating Rac1, our results are consistent with the previous findings and suggest that increased synaptic Rac1 activity contributes to the neoteny of human synapses. Moreover, RhoGEF proteins are enriched in the turquoise module associated with human cognitive function. Thus, our analysis provides molecular evidence that links synaptic neoteny to the evolution of human cognition.

Early synaptic connections before the third trimester are often transient stepping-stones toward functional synaptic circuits in mature brains (*53*). Surprisingly, genetic variations of PSD proteins specifically abundant at midgestation are associated with adolescent-onset psychiatric disorders. Given the dysregulation of late-stage synaptic proteins after the onset of these disorders, our findings highlight the importance of early synaptic connections for shaping neuronal wiring and higher-order brain functions of the mature brain.

There are several limitations to this study. Isolation of PSDs by subcellular fractionation can include contaminants from other cellular compartments or associated structures (*54*). We have therefore applied multistep orthogonal data filtering to minimize the effect of contamination. Additional independent validation such as proximity proteomics or immunogold labeling will further determine if the proteins reported here are *bona fide* PSD components. Moreover, alternative splicing and the isoforms they produce play a key role in regulating synapse development (*55*, *56*), but due to technical limitations, our proteomic analysis does not include quantifications at the isoform level. With the development of novel methods, future studies that determine developmental changes of the synaptic proteome at the isoform level across different brain regions and cell types will provide further insight into the mechanisms of brain development, evolution, and disease.

Reference

1. H. Y. Zoghbi, M. F. Bear, Synaptic Dysfunction in Neurodevelopmental Disorders Associated with Autism and Intellectual Disabilities. *Cold Spring Harb. Perspect. Biol.* **4**, a009886–a009886 (2012).
2. W. G. Frankle, J. Lerma, M. Laruelle, The synaptic hypothesis of Schizophrenia. *Neuron*. **39**, 205–216 (2003).
3. G. M. Shankar, D. M. Walsh, Alzheimer's disease: Synaptic dysfunction and Aβ. *Mol. Neurodegener.* **4**, 1–13 (2009).
4. M. Sheng, E. Kim, The postsynaptic organization of synapses. *Cold Spring Harb. Perspect. Biol.* **3** (2011), doi:10.1101/cshperspect.a005678.
5. A. Bayés, L. N. van de Lagemaat, M. O. Collins, M. D. R. Croning, I. R. Whittle, J. S. Choudhary, S. G. N. Grant, Characterization of the proteome, diseases and evolution of the human postsynaptic density. *Nat. Neurosci.* **14**, 19–21 (2011).
6. M. T. Swulius, Y. Kubota, A. Forest, M. N. Waxham, Structure and composition of the postsynaptic density during development. *J. Comp. Neurol.* **518**, 4243–4260 (2010).
7. G. L. Sell, S. L. Barrow, A. K. McAllister, in *Synapse Development and Maturation* (Elsevier, 2020; http://dx.doi.org/10.1016/B978-0-12-823672-7.00001-6), pp. 3–32.
8. R. S. Petralia, N. Sans, Y. X. Wang, R. J. Wenthold, Ontogeny of postsynaptic density proteins at glutamatergic synapses. *Mol. Cell. Neurosci.* **29**, 436–452 (2005).
9. J. Li, W. Zhang, H. Yang, D. P. Howrigan, B. Wilkinson, T. Souaiaia, O. V Evgrafov, G. Genovese, V. A. Clementel, J. C. Tudor, T. Abel, J. A. Knowles, B. M. Neale, K. Wang, F. Sun, M. P. Coba, Spatiotemporal profile of postsynaptic interactomes integrates components of complex brain disorders. *Nat. Neurosci.* **20**, 1150–1161 (2017).
10. K. M. Harris, F. E. Jensen, B. Tsao, Three-dimensional structure of dendritic spines and synapses in rat hippocampus (CA1) at postnatal day 15 and adult ages: implications for the maturation of synaptic physiology and long-term potentiation. *J. Neurosci.* **12**, 2685–705 (1992).
11. B. van Zundert, A. Yoshii, M. Constantine-Paton, Receptor compartmentalization and trafficking at glutamate synapses: a developmental proposal. *Trends Neurosci.* **27**, 428–

437 (2004).

12. G. M. Elias, L. A. B. Elias, P. F. Apostolides, A. R. Kriegstein, R. A. Nicoll, Differential trafficking of AMPA and NMDA receptors by SAP102 and PSD-95 underlies synapse development. *Proc. Natl. Acad. Sci. U. S. A.* **105**, 20953–20958 (2008).

13. J. A. Gray, Y. Shi, H. Usui, M. J. During, K. Sakimura, R. A. Nicoll, Distinct Modes of AMPA Receptor Suppression at Developing Synapses by GluN2A and GluN2B: Single-Cell NMDA Receptor Subunit Deletion In Vivo. *Neuron*. **71**, 1085–1101 (2011).

14. J. DeFelipe, The evolution of the brain, the human nature of cortical circuits, and intellectual creativity. *Front. Neuroanat.* **5**, 1–17 (2011).

15. G. N. Elston, R. Benavides-Piccione, J. DeFelipe, The pyramidal cell in cognition: a comparative study in human and monkey. *J. Neurosci.* **21**, 1–5 (2001).

16. À. Bayés, M. O. Collins, R. Reig-Viader, G. Gou, D. Goulding, A. Izquierdo, J. S. Choudhary, R. D. Emes, S. G. N. Grant, Evolution of complexity in the zebrafish synapse proteome. *Nat. Commun.* **8** (2017), doi:10.1038/ncomms14613.

17. À. Bayés, M. O. Collins, M. D. R. Croning, L. N. van de Lagemaat, J. S. Choudhary, S. G. N. Grant, Comparative Study of Human and Mouse Postsynaptic Proteomes Finds High Compositional Conservation and Abundance Differences for Key Synaptic Proteins. *PLoS One*. **7**, e46683 (2012).

18. R. D. Emes, A. J. Pocklington, C. N. G. Anderson, A. Bayes, M. O. Collins, C. A. Vickers, M. D. R. Croning, B. R. Malik, J. S. Choudhary, J. D. Armstrong, S. G. N. Grant, Evolutionary expansion and anatomical specialization of synapse proteome complexity. *Nat. Neurosci.* **11**, 799–806 (2008).

19. R. Benavides-Piccione, I. Ballesteros-Yáñez, J. DeFelipe, R. Yuste, Cortical area and species differences in dendritic spine morphology. *J. Neurocytol.* **31**, 337–346 (2002).

20. M. Shibata, K. Pattabiraman, S. K. Muchnik, N. Kaur, Y. M. Morozov, X. Cheng, S. G. Waxman, N. Sestan, Hominini-specific regulation of CBLN2 increases prefrontal spinogenesis. *Nature*. **598**, 489–494 (2021).

21. Z. Petanjek, M. Judas, G. Simic, M. R. Rasin, H. B. M. Uylings, P. Rakic, I. Kostovic, Extraordinary neoteny of synaptic spines in the human prefrontal cortex. *Proc. Natl. Acad. Sci.* **108**, 13281–13286 (2011).

22. X. Liu, M. Somel, L. Tang, Z. Yan, X. Jiang, S. Guo, Y. Yuan, L. He, A. Oleksiak, Y. Zhang, N. Li, Y. Hu, W. Chen, Z. Qiu, S. Pääbo, P. Khaitovich, Extension of cortical synaptic development distinguishes humans from chimpanzees and macaques. *Genome Res.* **22**, 611–622 (2012).

23. E. R. E. Schmidt, F. Polleux, Genetic Mechanisms Underlying the Evolution of Connectivity in the Human Cortex. *Front. Neural Circuits*. **15**, 1–16 (2022).

24. L. Wang, K. Pang, K. Han, C. J. Adamski, W. Wang, L. He, J. K. Lai, V. V. Bondar, J. G. Duman, R. Richman, K. F. Tolias, P. Barth, T. Palzkill, Z. Liu, J. L. Holder, H. Y. Zoghbi, An autism-linked missense mutation in SHANK3 reveals the modularity of Shank3 function. *Mol. Psychiatry*. **25**, 2534–2555 (2020).

25. À. Bayés, M. O. Collins, C. M. Galtrey, C. Simonnet, M. Roy, M. D. R. Croning, G. Gou, L. N. Van De Lagemaat, D. Milward, I. R. Whittle, C. Smith, J. S. Choudhary, S. G. N. Grant, Human post-mortem synapse proteome integrity screening for proteomic studies of postsynaptic complexes. *Mol. Brain*. **7**, 1–11 (2014).

26. M. Roy, O. Sorokina, N. Skene, C. Simonnet, F. Mazzo, R. Zwart, E. Sher, C. Smith, J. D. Armstrong, S. G. N. Grant, Proteomic analysis of postsynaptic proteins in regions of the human neocortex. *Nat. Neurosci.* **21**, 130–141 (2018).

27. L. Pickard, J. Noel, J. M. Henley, G. L. Collingridge, E. Molnar, Developmental changes in synaptic AMPA and NMDA receptor distribution and AMPA receptor subunit composition in living hippocampal neurons. *J. Neurosci.* **20**, 7922–7931 (2000).

28. P. Langfelder, S. Horvath, WGCNA: an R package for weighted correlation network analysis. *BMC Bioinformatics*. **9**, 559 (2008).

29. F. Koopmans, P. van Nierop, M. Andres-Alonso, A. Byrnes, T. Cijsouw, M. P. Coba, L. N. Cornelisse, R. J. Farrell, H. L. Goldschmidt, D. P. Howrigan, N. K. Hussain, C. Imig, A. P. H. de Jong, H. Jung, M. Kohansalnodehi, B. Kramarz, N. Lipstein, R. C. Lovering, H. MacGillavry, V. Mariano, H. Mi, M. Ninov, D. Osumi-Sutherland, R. Pielot, K.-H. Smalla, H. Tang, K. Tashman, R. F. G. Toonen, C. Verpelli, R. Reig-Viader, K. Watanabe, J. van Weering, T. Achsel, G. Ashrafi, N. Asi, T. C. Brown, P. De Camilli, M. Feuermann, R. E. Foulger, P. Gaudet, A. Joglekar, A. Kanellopoulos, R. Malenka, R. A. Nicoll, C. Pulido, J. de Juan-Sanz, M. Sheng, T. C. Südhof, H. U. Tilgner, C. Bagni, À. Bayés, T. Biederer, N. Brose, J. J. E. Chua, D. C. Dieterich, E. D. Gundelfinger, C. Hoogenraad, R. L. Huganir, R. Jahn, P. S. Kaeser, E. Kim, M. R. Kreutz, P. S. McPherson, B. M. Neale, V. O'Connor, D. Posthuma, T. A. Ryan, C. Sala, G. Feng, S. E. Hyman, P. D. Thomas, A. B. Smit, M. Verhage, SynGO: An Evidence-Based, Expert-Curated Knowledge Base for the Synapse. *Neuron*. **103**, 217-234.e4 (2019).

30. Y. Zhu, A. M. M. Sousa, T. Gao, M. Skarica, M. Li, G. Santpere, P. Esteller-Cucala, D. Juan, L. Ferrández-Peral, F. O. Gulden, M. Yang, D. J. Miller, T. Marques-Bonet, Y. Imamura Kawasawa, H. Zhao, N. Sestan, Spatiotemporal transcriptomic divergence across human and macaque brain development. *Science*. **362** (2018), doi:10.1126/science.aat8077.

31. M. Li, G. Santpere, Y. Imamura Kawasawa, O. V. Evgrafov, F. O. Gulden, S. Pochareddy, S. M. Sunkin, Z. Li, Y. Shin, Y. Zhu, A. M. M. Sousa, D. M. Werling, R. R. Kitchen, H. J. Kang, M. Pletikos, J. Choi, S. Muchnik, X. Xu, D. Wang, B. Lorente-Galdos, S. Liu, P. Giusti-Rodríguez, H. Won, C. A. de Leeuw, A. F. Pardiñas, BrainSpan Consortium, PsychENCODE Consortium, PsychENCODE Developmental Subgroup, M. Hu, F. Jin, Y. Li, M. J. Owen, M. C. O'Donovan, J. T. R. Walters, D. Posthuma, M. A. Reimers, P. Levitt, D. R. Weinberger, T. M. Hyde, J. E. Kleinman, D. H. Geschwind, M. J. Hawrylycz, M. W. State, S. J. Sanders, P. F. Sullivan, M. B. Gerstein, E. S. Lein, J. A. Knowles, N. Sestan, Integrative functional genomic analysis of human brain development and neuropsychiatric risks. *Science*. **362** (2018), doi:10.1126/science.aat7615.

32. P. Langfelder, R. Luo, M. C. Oldham, S. Horvath, Is my network module preserved and reproducible? *PLoS Comput. Biol.* **7**, e1001057 (2011).

33. A. Bhaduri, C. Sandoval-Espinosa, M. Otero-Garcia, I. Oh, R. Yin, U. C. Eze, T. J.

Nowakowski, A. R. Kriegstein, An atlas of cortical arealization identifies dynamic molecular signatures. *Nature*. **598**, 200–204 (2021).

34. T. E. Bakken, N. L. Jorstad, Q. Hu, B. B. Lake, W. Tian, B. E. Kalmbach, M. Crow, R. D. Hodge, F. M. Krienen, S. A. Sorensen, J. Eggermont, Z. Yao, B. D. Aevermann, A. I. Aldridge, A. Bartlett, D. Bertagnolli, T. Casper, R. G. Castanon, K. Crichton, T. L. Daigle, R. Dalley, N. Dee, N. Dembrow, D. Diep, S. L. Ding, W. Dong, R. Fang, S. Fischer, M. Goldman, J. Goldy, L. T. Graybuck, B. R. Herb, X. Hou, J. Kancherla, M. Kroll, K. Lathia, B. van Lew, Y. E. Li, C. S. Liu, H. Liu, J. D. Lucero, A. Mahurkar, D. McMillen, J. A. Miller, M. Moussa, J. R. Nery, P. R. Nicovich, S. Y. Niu, J. Orvis, J. K. Osteen, S. Owen, C. R. Palmer, T. Pham, N. Plongthongkum, O. Poirion, N. M. Reed, C. Rimorin, A. Rivkin, W. J. Romanow, A. E. Sedeño-Cortés, K. Siletti, S. Somasundaram, J. Sulc, M. Tieu, A. Torkelson, H. Tung, X. Wang, F. Xie, A. M. Yanny, R. Zhang, S. A. Ament, M. M. Behrens, H. C. Bravo, J. Chun, A. Dobin, J. Gillis, R. Hertzano, P. R. Hof, T. Höllt, G. D. Horwitz, C. D. Keene, P. V. Kharchenko, A. L. Ko, B. P. Lelieveldt, C. Luo, E. A. Mukamel, A. Pinto-Duarte, S. Preissl, A. Regev, B. Ren, R. H. Scheuermann, K. Smith, W. J. Spain, O. R. White, C. Koch, M. Hawrylycz, B. Tasic, E. Z. Macosko, S. A. McCarroll, J. T. Ting, H. Zeng, K. Zhang, G. Feng, J. R. Ecker, S. Linnarsson, E. S. Lein, Comparative cellular analysis of motor cortex in human, marmoset and mouse. *Nature*. **598**, 111–119 (2021).

35. L. J. Wu, X. Li, T. Chen, M. Ren, M. Zhuo, Characterization of intracortical synaptic connections in the mouse anterior cingulate cortex using dual patch clamp recording. *Mol. Brain*. **2**, 1–12 (2009).

36. S. Loomba, J. Straehle, V. Gangadharan, N. Heike, A. Khalifa, A. Motta, N. Ju, M. Sievers, J. Gempt, H. S. Meyer, M. Helmstaedter, Connectomic comparison of mouse and human cortex. *Science*. **377**, eabo0924 (2022).

37. A. D. Workman, C. J. Charvet, B. Clancy, R. B. Darlington, B. L. Finlay, Modeling transformations of neurodevelopmental sequences across mammalian species. *J. Neurosci.* **33**, 7368–7383 (2013).

38. R. K. Carlin, D. J. Grab, P. Siekevitz, Postmortem Accumulation of Tubulin in Postsynaptic Density Preparations. *J. Neurochem.* **38**, 94–100 (1982).

39. C. T. Schanzenbächer, J. D. Langer, E. M. Schuman, Time- and polarity-dependent proteomic changes associated with homeostatic scaling at central synapses. *Elife*. **7**, 1–20 (2018).

40. A. Y. Hung, C. C. Sung, I. L. Brito, M. Sheng, Degradation of postsynaptic scaffold GKAP and regulation of dendritic spine morphology by the TRIM3 ubiquitin ligase in rat hippocampal neurons. *PLoS One*. **5**, e9842 (2010).

41. S.-L. Chiu, G. H. Diering, B. Ye, K. Takamiya, C.-M. Chen, Y. Jiang, T. Niranjan, C. E. Schwartz, T. Wang, R. L. Huganir, GRASP1 Regulates Synaptic Plasticity and Learning through Endosomal Recycling of AMPA Receptors. *Neuron*. **93**, 1405-1419.e8 (2017).

42. R. Ben-Shalom, C. M. Keeshen, K. N. Berrios, J. Y. An, S. J. Sanders, K. J. Bender, Opposing Effects on NaV1.2 Function Underlie Differences Between SCN2A Variants Observed in Individuals With Autism Spectrum Disorder or Infantile Seizures. *Biol. Psychiatry*. **82**, 224–232 (2017).

43. C. K. Cheon, S. H. Lim, Y. M. Kim, D. Kim, N. Y. Lee, T. S. Yoon, N. S. Kim, E. Kim, J. R. Lee, Autosomal dominant transmission of complicated hereditary spastic paraplegia due to a dominant negative mutation of KIF1A, SPG30 gene. *Sci. Rep.* **7**, 1–11 (2017).

44. M. Cizeron, Z. Qiu, B. Koniaris, R. Gokhale, N. H. Komiyama, E. Fransén, S. G. N. Grant, A brainwide atlas of synapses across the mouse life span. *Science*. **369**, 270–275 (2020).

45. F. Polleux, G. Ince-Dunn, A. Ghosh, Transcriptional regulation of vertebrate axon guidance and synapse formation. *Nat. Rev. Neurosci.* **8**, 331–340 (2007).

46. F. Zhu, M. O. Collins, J. Harmse, J. S. Choudhary, S. G. N. Grant, N. H. Komiyama, Cell-type-specific visualisation and biochemical isolation of endogenous synaptic proteins in mice. *Eur. J. Neurosci.* **51**, 793–805 (2020).

47. W. Zhang, L. Vazquez, M. Apperson, M. B. Kennedy, Citron binds to PSD-95 at glutamatergic synapses on inhibitory neurons in the hippocampus. *J. Neurosci.* **19**, 96–108 (1999).

48. A. M. Bygrave, A. Sengupta, E. P. Jackert, M. Ahmed, B. Adenuga, H. L. Goldschmidt, R. C. Johnson, H. Zhong, F. L. Yeh, M. Sheng, R. L. Huganir, *bioRxiv*, in press, doi:10.1101/2021.11.01.466782.

49. J. D. Perez, S. Tom Dieck, B. Alvarez-Castelao, G. Tushev, I. C. W. Chan, E. M. Schuman, Subcellular sequencing of single neurons reveals the dendritic transcriptome of gabaergic interneurons. *Elife*. **10**, 1–26 (2021).

50. C. Charrier, K. Joshi, J. Coutinho-Budd, J. E. Kim, N. Lambert, J. De Marchena, W. L. Jin, P. Vanderhaeghen, A. Ghosh, T. Sassa, F. Polleux, Inhibition of SRGAP2 function by its human-specific paralogs induces neoteny during spine maturation. *Cell*. **149**, 923–935 (2012).

51. M. Fossati, R. Pizzarelli, E. R. Schmidt, J. V. Kupferman, D. Stroebel, F. Polleux, C. Charrier, SRGAP2 and Its Human-Specific Paralog Co-Regulate the Development of Excitatory and Inhibitory Synapses. *Neuron*. **91**, 356–369 (2016).

52. E. R. E. Schmidt, H. T. Zhao, J. M. Park, M. Dipoppa, M. M. Monsalve-Mercado, J. B. Dahan, C. C. Rodgers, A. Lejeune, E. M. C. Hillman, K. D. Miller, R. M. Bruno, F. Polleux, A human-specific modifier of cortical connectivity and circuit function. *Nature*. **599**, 640–644 (2021).

53. G. Z. Tau, B. S. Peterson, Normal Development of Brain Circuits. *Neuropsychopharmacology*. **35**, 147–168 (2010).

54. R. K. Carlin, D. J. Grab, R. S. Cohen, P. Siekevitz, Isolation and characterization of postsynaptic densities from various brain regions: Enrichment of different types of postsynaptic densities. *J. Cell Biol.* **86**, 831–843 (1980).

55. L. Traunmüller, A. M. Gomez, T.-M. Nguyen, P. Scheiffele, Control of neuronal synapse specification by a highly dedicated alternative splicing program. *Science*. **352**, 982–6 (2016).

56. J. Dai, J. Aoto, T. C. Südhof, Alternative Splicing of Presynaptic Neurexins Differentially Controls Postsynaptic NMDA and AMPA Receptor Responses. *Neuron*. **102**, 993-1008.e5

(2019).

57. J. Cox, M. Mann, MaxQuant enables high peptide identification rates, individualized p.p.b.-range mass accuracies and proteome-wide protein quantification. *Nat. Biotechnol.* **26**, 1367–1372 (2008).

58. B. Schwanhüusser, D. Busse, N. Li, G. Dittmar, J. Schuchhardt, J. Wolf, W. Chen, M. Selbach, Global quantification of mammalian gene expression control. *Nature*. **473**, 337–342 (2011).

59. S. Rath, R. Sharma, R. Gupta, T. Ast, C. Chan, T. J. Durham, R. P. Goodman, Z. Grabarek, M. E. Haas, W. H. W. Hung, P. R. Joshi, A. A. Jourdain, S. H. Kim, A. V. Kotrys, S. S. Lam, J. G. McCoy, J. D. Meisel, M. Miranda, A. Panda, A. Patgiri, R. Rogers, S. Sadre, H. Shah, O. S. Skinner, T. L. To, M. A. Walker, H. Wang, P. S. Ward, J. Wengrod, C. C. Yuan, S. E. Calvo, V. K. Mootha, MitoCarta3.0: An updated mitochondrial proteome now with sub-organelle localization and pathway annotations. *Nucleic Acids Res.* **49**, D1541–D1547 (2021).

60. R. S. Walikonis, O. N. Jensen, M. Mann, D. W. Provance, J. A. Mercer, M. B. Kennedy, Identification of proteins in the postsynaptic density fraction by mass spectrometry. *J. Neurosci.* **20**, 4069–4080 (2000).

61. J. B. Shin, J. F. Krey, A. Hassan, Z. Metlagel, A. N. Tauscher, J. M. Pagana, N. E. Sherman, E. D. Jeffery, K. J. Spinelli, H. Zhao, P. A. Wilmarth, D. Choi, L. L. David, M. Auer, P. G. Barr-Gillespie, Molecular architecture of the chick vestibular hair bundle. *Nat. Neurosci.* **16**, 365–374 (2013).

62. X. Zhang, A. H. Smits, G. B. A. Van Tilburg, H. Ovaa, W. Huber, M. Vermeulen, Proteome-wide identification of ubiquitin interactions using UbIA-MS. *Nat. Protoc.* **13**, 530–550 (2018).

63. M. E. Ritchie, B. Phipson, D. Wu, Y. Hu, C. W. Law, W. Shi, G. K. Smyth, Limma powers differential expression analyses for RNA-sequencing and microarray studies. *Nucleic Acids Res.* **43**, e47 (2015).

64. Y. Benjamini, Y. Hochberg, Controlling the False Discovery Rate : A Practical and Powerful Approach to Multiple Testing. *J. R. Stat. Soc.* **57**, 289–300 (1995).

65. Z. Gu, R. Eils, M. Schlesner, Complex heatmaps reveal patterns and correlations in multidimensional genomic data. *Bioinformatics*. **32**, 2847–2849 (2016).

66. G. E. Hoffman, E. E. Schadt, variancePartition: Interpreting drivers of variation in complex gene expression studies. *BMC Bioinformatics*. **17**, 17–22 (2016).

67. A. Subramanian, P. Tamayo, V. K. Mootha, S. Mukherjee, B. L. Ebert, M. A. Gillette, A. Paulovich, S. L. Pomeroy, T. R. Golub, E. S. Lander, J. P. Mesirov, Gene set enrichment analysis: A knowledge-based approach for interpreting genome-wide expression profiles. *Proc. Natl. Acad. Sci. U. S. A.* **102**, 15545–15550 (2005).

68. G. Yu, L. G. Wang, Y. Han, Q. Y. He, ClusterProfiler: An R package for comparing biological themes among gene clusters. *Omi. A J. Integr. Biol.* **16**, 284–287 (2012).

69. A. Liberzon, C. Birger, H. Thorvaldsdóttir, M. Ghandi, J. P. Mesirov, P. Tamayo, The Molecular Signatures Database Hallmark Gene Set Collection. *Cell Syst.* **1**, 417–425

(2015).

70. J. Schindelin, I. Arganda-Carreras, E. Frise, V. Kaynig, M. Longair, T. Pietzsch, S. Preibisch, C. Rueden, S. Saalfeld, B. Schmid, J. Y. Tinevez, D. J. White, V. Hartenstein, K. Eliceiri, P. Tomancak, A. Cardona, Fiji: An open-source platform for biological-image analysis. *Nat. Methods*. **9**, 676–682 (2012).

71. C. Stark, B. J. Breitkreutz, T. Reguly, L. Boucher, A. Breitkreutz, M. Tyers, BioGRID: a general repository for interaction datasets. *Nucleic Acids Res.* **34**, 535–539 (2006).

72. P. Shannon, A. Markiel, O. Ozier, N. S. Baliga, J. T. Wang, D. Ramage, N. Amin, B. Schwikowski, T. Ideker, Cytoscape: a software environment for integrated models of biomolecular interaction networks. *Genome Res.* **13**, 2498–504 (2003).

73. G. Csardi, T. Nepusz, The igraph software package for complex network research. *InterJournal Complex Syst.* (2006) (available at http://igraph.sf.net).

74. I. Letunic, S. Khedkar, P. Bork, SMART: Recent updates, new developments and status in 2020. *Nucleic Acids Res.* **49**, D458–D460 (2021).

75. S. N. Wood, Fast stable restricted maximum likelihood and marginal likelihood estimation of semiparametric generalized linear models. *J. R. Stat. Soc. Ser. B Stat. Methodol.* **73**, 3–36 (2011).

76. A. B. Keenan, D. Torre, A. Lachmann, A. K. Leong, M. L. Wojciechowicz, V. Utti, K. M. Jagodnik, E. Kropiwnicki, Z. Wang, A. Ma'ayan, ChEA3: transcription factor enrichment analysis by orthogonal omics integration. *Nucleic Acids Res.* **47**, W212–W224 (2019).

77. C. Hafemeister, R. Satija, Normalization and variance stabilization of single-cell RNA-seq data using regularized negative binomial regression. *Genome Biol.* **20**, 1–15 (2019).

78. Y. Hao, S. Hao, E. Andersen-Nissen, W. M. Mauck, S. Zheng, A. Butler, M. J. Lee, A. J. Wilk, C. Darby, M. Zager, P. Hoffman, M. Stoeckius, E. Papalexi, E. P. Mimitou, J. Jain, A. Srivastava, T. Stuart, L. M. Fleming, B. Yeung, A. J. Rogers, J. M. McElrath, C. A. Blish, R. Gottardo, P. Smibert, R. Satija, Integrated analysis of multimodal single-cell data. *Cell*. **184**, 3573-3587.e29 (2021).

79. M. L. Speir, B. Aparna, N. S. Markov, P. Moreno, T. J. Nowakowski, I. Papatheodorou, A. A. Pollen, L. Seninge, W. James Kent, M. Haeussler, *bioRxiv*, in press (available at https://doi.org/10.1101/2020.10.30.361162).

80. J. Friedman, T. Hastie, R. Tibshirani, Regularization Paths for Generalized Linear Models via Coordinate Descent. *J. Stat. Softw.* **33**, 1–22 (2010).

81. C. A. de Leeuw, J. M. Mooij, T. Heskes, D. Posthuma, MAGMA: Generalized Gene-Set Analysis of GWAS Data. *PLoS Comput. Biol.* **11**, 1–19 (2015).

82. K. Watanabe, S. Stringer, O. Frei, M. Umićević Mirkov, C. de Leeuw, T. J. C. Polderman, S. van der Sluis, O. A. Andreassen, B. M. Neale, D. Posthuma, A global overview of pleiotropy and genetic architecture in complex traits. *Nat. Genet.* **51**, 1339–1348 (2019).

83. K. J. Karczewski, L. C. Francioli, G. Tiao, B. B. Cummings, J. Alföldi, Q. Wang, R. L. Collins, K. M. Laricchia, A. Ganna, D. P. Birnbaum, L. D. Gauthier, H. Brand, M. Solomonson, N. A. Watts, D. Rhodes, M. Singer-Berk, E. M. England, E. G. Seaby, J. A.

Kosmicki, R. K. Walters, K. Tashman, Y. Farjoun, E. Banks, T. Poterba, A. Wang, C. Seed, N. Whiffin, J. X. Chong, K. E. Samocha, E. Pierce-Hoffman, Z. Zappala, A. H. O'Donnell-Luria, E. V. Minikel, B. Weisburd, M. Lek, J. S. Ware, C. Vittal, I. M. Armean, L. Bergelson, K. Cibulskis, K. M. Connolly, M. Covarrubias, S. Donnelly, S. Ferriera, S. Gabriel, J. Gentry, N. Gupta, T. Jeandet, D. Kaplan, C. Llanwarne, R. Munshi, S. Novod, N. Petrillo, D. Roazen, V. Ruano-Rubio, A. Saltzman, M. Schleicher, J. Soto, K. Tibbetts, C. Tolonen, G. Wade, M. E. Talkowski, C. A. Aguilar Salinas, T. Ahmad, C. M. Albert, D. Ardissino, G. Atzmon, J. Barnard, L. Beaugerie, E. J. Benjamin, M. Boehnke, L. L. Bonnycastle, E. P. Bottinger, D. W. Bowden, M. J. Bown, J. C. Chambers, J. C. Chan, D. Chasman, J. Cho, M. K. Chung, B. Cohen, A. Correa, D. Dabelea, M. J. Daly, D. Darbar, R. Duggirala, J. Dupuis, P. T. Ellinor, R. Elosua, J. Erdmann, T. Esko, M. Färkkilä, J. Florez, A. Franke, G. Getz, B. Glaser, S. J. Glatt, D. Goldstein, C. Gonzalez, L. Groop, C. Haiman, C. Hanis, M. Harms, M. Hiltunen, M. M. Holi, C. M. Hultman, M. Kallela, J. Kaprio, S. Kathiresan, B. J. Kim, Y. J. Kim, G. Kirov, J. Kooner, S. Koskinen, H. M. Krumholz, S. Kugathasan, S. H. Kwak, M. Laakso, T. Lehtimäki, R. J. F. Loos, S. A. Lubitz, R. C. W. Ma, D. G. MacArthur, J. Marrugat, K. M. Mattila, S. McCarroll, M. I. McCarthy, D. McGovern, R. McPherson, J. B. Meigs, O. Melander, A. Metspalu, B. M. Neale, P. M. Nilsson, M. C. O'Donovan, D. Ongur, L. Orozco, M. J. Owen, C. N. A. Palmer, A. Palotie, K. S. Park, C. Pato, A. E. Pulver, N. Rahman, A. M. Remes, J. D. Rioux, S. Ripatti, D. M. Roden, D. Saleheen, V. Salomaa, N. J. Samani, J. Scharf, H. Schunkert, M. B. Shoemaker, P. Sklar, H. Soininen, H. Sokol, T. Spector, P. F. Sullivan, J. Suvisaari, E. S. Tai, Y. Y. Teo, T. Tiinamaija, M. Tsuang, D. Turner, T. Tusie-Luna, E. Vartiainen, H. Watkins, R. K. Weersma, M. Wessman, J. G. Wilson, R. J. Xavier, B. M. Neale, M. J. Daly, D. G. MacArthur, The mutational constraint spectrum quantified from variation in 141,456 humans. *Nature*. **581**, 434–443 (2020).

84. T. N. Turner, Q. Yi, N. Krumm, J. Huddleston, K. Hoekzema, H. A. F. Stessman, A.-L. Doebley, R. A. Bernier, D. A. Nickerson, E. E. Eichler, denovo-db: a compendium of human de novo variants. *Nucleic Acids Res.* **45**, D804–D811 (2017).

85. H. O. Heyne, T. Singh, H. Stamberger, R. Abou Jamra, H. Caglayan, D. Craiu, P. De Jonghe, R. Guerrini, K. L. Helbig, B. P. C. Koeleman, J. A. Kosmicki, T. Linnankivi, P. May, H. Muhle, R. S. Møller, B. A. Neubauer, A. Palotie, M. Pendziwiat, P. Striano, S. Tang, S. Wu, A. Poduri, Y. G. Weber, S. Weckhuysen, S. M. Sisodiya, M. J. Daly, I. Helbig, D. Lal, J. R. Lemke, De novo variants in neurodevelopmental disorders with epilepsy. *Nat. Genet.* **50**, 1048–1053 (2018).

86. E. Rees, J. Han, J. Morgan, N. Carrera, V. Escott-Price, A. J. Pocklington, M. Duffield, L. S. Hall, S. E. Legge, A. F. Pardiñas, A. L. Richards, J. Roth, T. Lezheiko, N. Kondratyev, V. Kaleda, V. Golimbet, M. Parellada, J. González-Peñas, C. Arango, B. Z. Alizadeh, T. van Amelsvoort, R. Bruggeman, W. Cahn, L. de Haan, J. J. Luykx, B. P. F. Rutten, J. van Os, R. van Winkel, M. Gawlik, G. Kirov, J. T. R. Walters, P. Holmans, M. C. O'Donovan, M. J. Owen, De novo mutations identified by exome sequencing implicate rare missense variants in SLC6A1 in schizophrenia. *Nat. Neurosci.* **23**, 179–184 (2020).

87. D. P. Howrigan, S. A. Rose, K. E. Samocha, M. Fromer, F. Cerrato, W. J. Chen, C. Churchhouse, K. Chambert, S. D. Chandler, M. J. Daly, A. Dumont, G. Genovese, H. G. Hwu, N. Laird, J. A. Kosmicki, J. L. Moran, C. Roe, T. Singh, S. H. Wang, S. V. Faraone, S. J. Glatt, S. A. McCarroll, M. Tsuang, B. M. Neale, Exome sequencing in

schizophrenia-affected parent–offspring trios reveals risk conferred by protein-coding de novo mutations. *Nat. Neurosci.* **23**, 185–193 (2020).

88. D. M. Ruderfer, S. Ripke, A. McQuillin, J. Boocock, E. A. Stahl, J. M. W. Pavlides, N. Mullins, A. W. Charney, A. P. S. Ori, L. M. O. Loohuis, E. Domenici, A. Di Florio, S. Papiol, J. L. Kalman, V. Trubetskoy, R. Adolfsson, I. Agartz, E. Agerbo, H. Akil, D. Albani, M. Albus, M. Alda, M. Alexander, N. Alliey-Rodriguez, T. D. Als, F. Amin, A. Anjorin, M. J. Arranz, S. Awasthi, S. A. Bacanu, J. A. Badner, M. Baekvad-Hansen, S. Bakker, G. Band, J. D. Barchas, I. Barroso, N. Bass, M. Bauer, B. T. Baune, M. Begemann, C. Bellenguez, R. A. Belliveau, F. Bellivier, S. Bender, J. Bene, S. E. Bergen, W. H. Berrettini, E. Bevilacqua, J. M. Biernacka, T. B. Bigdeli, D. W. Black, H. Blackburn, J. M. Blackwell, D. H. R. Blackwood, C. B. Pedersen, M. Boehnke, M. Boks, A. D. Borglum, E. Bramon, G. Breen, M. A. Brown, R. Bruggeman, N. G. Buccola, R. L. Buckner, M. Budde, B. Bulik-Sullivan, S. J. Bumpstead, W. Bunney, M. Burmeister, J. D. Buxbaum, J. Bybjerg-Grauholm, W. Byerley, W. Cahn, G. Cai, M. J. Cairns, D. Campion, R. M. Cantor, V. J. Carr, N. Carrera, J. P. Casas, M. Casas, S. V. Catts, P. Cervantes, K. D. Chambert, R. C. K. Chan, E. Y. H. Chen, R. Y. L. Chen, W. Cheng, E. F. C. Cheung, S. A. Chong, T. K. Clarke, C. R. Cloninger, D. Cohen, N. Cohen, J. R. I. Coleman, D. A. Collier, P. Cormican, W. Coryell, N. Craddock, D. W. Craig, B. Crespo-Facorro, J. J. Crowley, C. Cruceanu, D. Curtis, P. M. Czerski, A. M. Dale, M. J. Daly, U. Dannlowski, A. Darvasi, M. Davidson, K. L. Davis, C. A. de Leeuw, F. Degenhardt, J. Del Favero, L. E. DeLisi, P. Deloukas, D. Demontis, J. R. DePaulo, M. di Forti, D. Dikeos, T. Dinan, S. Djurovic, A. L. Dobbyn, P. Donnelly, G. Donohoe, E. Drapeau, S. Dronov, J. Duan, F. Dudbridge, A. Duncanson, H. Edenberg, S. Edkins, H. Ehrenreich, P. Eichhammer, T. Elvsashagen, J. Eriksson, V. Escott-Price, T. Esko, L. Essioux, B. Etain, C. C. Fan, K. H. Farh, M. S. Farrell, M. Flickinger, T. M. Foroud, L. Forty, J. Frank, L. Franke, C. Fraser, R. Freedman, C. Freeman, N. B. Freimer, J. I. Friedman, M. Fromer, M. A. Frye, J. M. Fullerton, K. Gade, J. Garnham, H. A. Gaspar, P. V. Gejman, G. Genovese, L. Georgieva, C. Giambartolomei, E. Giannoulatou, I. Giegling, M. Gill, M. Gillman, M. G. Pedersen, P. Giusti-Rodriguez, S. Godard, F. Goes, J. I. Goldstein, S. Gopal, S. D. Gordon, K. Gordon-Smith, J. Gratten, E. Gray, E. K. Green, M. J. Green, T. A. Greenwood, M. Grigoroiu-Serbanescu, J. Grove, W. Guan, H. Gurling, J. G. Parra, R. Gwilliam, L. de Haan, J. Hall, M. H. Hall, C. Hammer, N. Hammond, M. L. Hamshere, M. Hansen, T. Hansen, V. Haroutunian, A. M. Hartmann, J. Hauser, M. Hautzinger, U. Heilbronner, G. Hellenthal, F. A. Henskens, S. Herms, M. Hipolito, J. N. Hirschhorn, P. Hoffmann, M. V. Hollegaard, D. M. Hougaard, H. Huang, L. Huckins, C. M. Hultman, S. E. Hunt, M. Ikeda, N. Iwata, C. Iyegbe, A. V. Jablensky, S. Jamain, J. Jankowski, A. Jayakumar, I. Joa, I. Jones, L. A. Jones, E. G. Jonsson, A. Julia, A. Jureus, A. K. Kahler, R. S. Kahn, L. Kalaydjieva, R. Kandaswamy, S. Karachanak-Yankova, J. Karjalainen, R. Karlsson, D. Kavanagh, M. C. Keller, B. J. Kelly, J. Kelsoe, J. L. Kennedy, A. Khrunin, Y. Kim, G. Kirov, S. Kittel-Schneider, J. Klovins, J. Knight, S. V. Knott, J. A. Knowles, M. Kogevinas, B. Konte, E. Kravariti, V. Kucinskas, Z. A. Kucinskiene, R. Kupka, H. Kuzelova-Ptackova, M. Landen, C. Langford, C. Laurent, J. Lawrence, S. Lawrie, W. B. Lawson, M. Leber, M. Leboyer, P. H. Lee, J. L. C. Keong, S. E. Legge, T. Lencz, B. Lerer, D. F. Levinson, S. E. Levy, C. M. Lewis, J. Z. Li, M. Li, Q. S. Li, T. Li, K. Y. Liang, J. Liddle, J. Lieberman, S. Limborska, K. Lin, D. H. Linszen, J. Lissowska, C. Liu, J. Liu, J. Lonnqvist, C. M. Loughland, J. Lubinski, S. Lucae, M. Macek, D. J. MacIntyre, P. K. E. Magnusson, B. S.

Maher, P. B. Mahon, W. Maier, A. K. Malhotra, J. Mallet, U. F. Malt, H. S. Markus, S. Marsal, N. G. Martin, I. Mata, C. G. Mathew, M. Mattheisen, M. Mattingsdal, F. Mayoral, O. T. McCann, R. W. McCarley, S. A. McCarroll, M. I. McCarthy, C. McDonald, S. L. McElroy, P. McGuffin, M. G. McInnis, A. M. McIntosh, J. D. McKay, F. J. McMahon, H. Medeiros, S. E. Medland, S. Meier, C. J. Meijer, B. Melegh, I. Melle, F. Meng, R. I. Mesholam-Gately, A. Metspalu, P. T. Michie, L. Milani, V. Milanova, P. B. Mitchell, Y. Mokrab, G. W. Montgomery, J. L. Moran, G. Morken, D. W. Morris, O. Mors, P. B. Mortensen, B. J. Mowry, T. W. Mühleisen, B. Müller-Myhsok, K. C. Murphy, R. M. Murray, R. M. Myers, I. Myin-Germeys, B. M. Neale, M. Nelis, I. Nenadic, D. A. Nertney, G. Nestadt, K. K. Nicodemus, C. M. Nievergelt, L. Nikitina-Zake, V. Nimgaonkar, L. Nisenbaum, M. Nordentoft, A. Nordin, M. M. Nöthen, E. A. Nwulia, E. O'Callaghan, C. O'Donovan, C. O'Dushlaine, F. A. O'Neill, K. J. Oedegaard, S. Y. Oh, A. Olincy, L. Olsen, L. Oruc, J. Van Os, M. J. Owen, S. A. Paciga, C. N. A. Palmer, A. Palotie, C. Pantelis, G. N. Papadimitriou, E. Parkhomenko, C. Pato, M. T. Pato, T. Paunio, R. Pearson, D. O. Perkins, R. H. Perlis, A. Perry, T. H. Pers, T. L. Petryshen, A. Pfennig, M. Picchioni, O. Pietilainen, J. Pimm, M. Pirinen, R. Plomin, A. J. Pocklington, D. Posthuma, J. B. Potash, S. C. Potter, J. Powell, A. Price, A. E. Pulver, S. M. Purcell, D. Quested, J. A. Ramos-Quiroga, H. B. Rasmussen, A. Rautanen, R. Ravindrarajah, E. J. Regeer, A. Reichenberg, A. Reif, M. A. Reimers, M. Ribases, J. P. Rice, A. L. Richards, M. Ricketts, B. P. Riley, F. Rivas, M. Rivera, J. L. Roffman, G. A. Rouleau, P. Roussos, D. Rujescu, V. Salomaa, C. Sanchez-Mora, A. R. Sanders, S. J. Sawcer, U. Schall, A. F. Schatzberg, W. A. Scheftner, P. R. Schofield, N. J. Schork, S. G. Schwab, E. M. Scolnick, L. J. Scott, R. J. Scott, L. J. Seidman, A. Serretti, P. C. Sham, C. S. Weickert, T. Shehktman, J. Shi, P. D. Shilling, E. Sigurdsson, J. M. Silverman, K. Sim, C. Slaney, P. Slominsky, O. B. Smeland, J. W. Smoller, H. C. So, J. L. Sobell, E. Soderman, C. S. Hansen, C. C. A. Spencer, A. T. Spijker, D. St Clair, H. Stefansson, K. Stefansson, S. Steinberg, E. Stogmann, E. Stordal, A. Strange, R. E. Straub, J. S. Strauss, F. Streit, E. Strengman, J. Strohmaier, T. S. Stroup, Z. Su, M. Subramaniam, J. Suvisaari, D. M. Svrakic, J. P. Szatkiewicz, S. Szelinger, A. Tashakkori-Ghanbaria, S. Thirumalai, R. C. Thompson, T. E. Thorgeirsson, D. Toncheva, P. A. Tooney, S. Tosato, T. Toulopoulou, R. C. Trembath, J. Treutlein, G. Turecki, A. E. Vaaler, H. Vedder, E. Vieta, J. Vincent, P. M. Visscher, A. C. Viswanathan, D. Vukcevic, J. Waddington, M. Waller, D. Walsh, M. Walshe, J. T. R. Walters, D. Wang, Q. Wang, W. Wang, Y. Wang, S. J. Watson, B. T. Webb, T. W. Weickert, D. R. Weinberger, M. Weisbrod, M. Weiser, T. Werge, P. Weston, P. Whittaker, S. Widaa, D. Wiersma, D. B. Wildenauer, N. M. Williams, S. Williams, S. H. Witt, A. R. Wolen, E. H. M. Wong, N. W. Wood, B. K. Wormley, J. Q. Wu, S. Xi, W. Xu, A. H. Young, C. C. Zai, P. Zandi, P. Zhang, X. Zheng, F. Zimprich, S. Zollner, A. Corvin, A. H. Fanous, S. Cichon, M. Rietschel, E. S. Gershon, T. G. Schulze, A. B. Cuellar-Barboza, A. J. Forstner, P. A. Holmans, J. I. Nurnberger, O. A. Andreassen, S. H. Lee, M. C. O'Donovan, P. F. Sullivan, R. A. Ophoff, N. R. Wray, P. Sklar, K. S. Kendler, Genomic Dissection of Bipolar Disorder and Schizophrenia, Including 28 Subphenotypes. *Cell*. **173**, 1705-1715.e16 (2018).

89. J. Grove, S. Ripke, T. D. Als, M. Mattheisen, R. K. Walters, H. Won, J. Pallesen, E. Agerbo, O. A. Andreassen, R. Anney, S. Awashti, R. Belliveau, F. Bettella, J. D. Buxbaum, J. Bybjerg-Grauholm, M. Bækvad-Hansen, F. Cerrato, K. Chambert, J. H. Christensen, C. Churchhouse, K. Dellenvall, D. Demontis, S. De Rubeis, B. Devlin, S.

Djurovic, A. L. Dumont, J. I. Goldstein, C. S. Hansen, M. E. Hauberg, M. V. Hollegaard, S. Hope, D. P. Howrigan, H. Huang, C. M. Hultman, L. Klei, J. Maller, J. Martin, A. R. Martin, J. L. Moran, M. Nyegaard, T. Nærland, D. S. Palmer, A. Palotie, C. B. Pedersen, M. G. Pedersen, T. dPoterba, J. B. Poulsen, B. S. Pourcain, P. Qvist, K. Rehnström, A. Reichenberg, J. Reichert, E. B. Robinson, K. Roeder, P. Roussos, E. Saemundsen, S. Sandin, F. K. Satterstrom, G. Davey Smith, H. Stefansson, S. Steinberg, C. R. Stevens, P. F. Sullivan, P. Turley, G. B. Walters, X. Xu, N. R. Wray, M. Trzaskowski, E. M. Byrne, A. Abdellaoui, M. J. Adams, T. M. Air, T. F. M. Andlauer, S. A. Bacanu, A. T. F. Beekman, T. B. Bigdeli, E. B. Binder, D. H. R. Blackwood, J. Bryois, H. N. Buttenschøn, N. Cai, E. Castelao, T. K. Clarke, J. R. I. Coleman, L. Colodro-Conde, B. Couvy-Duchesne, N. Craddock, G. E. Crawford, G. Davies, I. J. Deary, F. Degenhardt, E. M. Derks, N. Direk, C. V. Dolan, E. C. Dunn, T. C. Eley, V. Escott-Price, F. F. H. Kiadeh, H. K. Finucane, A. J. Forstner, J. Frank, H. A. Gaspar, M. Gill, F. S. Goes, S. D. Gordon, L. S. Hall, T. F. Hansen, S. Herms, I. B. Hickie, P. Hoffmann, G. Homuth, C. Horn, J. J. Hottenga, M. Ising, R. Jansen, E. Jorgenson, J. A. Knowles, I. S. Kohane, J. Kraft, W. W. Kretzschmar, J. Krogh, Z. Kutalik, Y. Li, P. A. Lind, D. J. MacIntyre, D. F. MacKinnon, R. M. Maier, W. Maier, J. Marchini, H. Mbarek, P. McGrath, P. McGuffin, S. E. Medland, D. Mehta, C. M. Middeldorp, E. Mihailov, Y. Milaneschi, L. Milani, F. M. Mondimore, G. W. Montgomery, S. Mostafavi, N. Mullins, M. Nauck, B. Ng, M. G. Nivard, D. R. Nyholt, P. F. O'Reilly, H. Oskarsson, M. J. Owen, J. N. Painter, R. E. Peterson, E. Pettersson, W. J. Peyrot, G. Pistis, D. Posthuma, J. A. Quiroz, J. P. Rice, B. P. Riley, M. Rivera, S. S. Mirza, R. Schoevers, E. C. Schulte, L. Shen, J. Shi, S. I. Shyn, E. Sigurdsson, G. C. B. Sinnamon, J. H. Smit, D. J. Smith, F. Streit, J. Strohmaier, K. E. Tansey, H. Teismann, A. Teumer, W. Thompson, P. A. Thomson, T. E. Thorgeirsson, M. Traylor, J. Treutlein, V. Trubetskoy, A. G. Uitterlinden, D. Umbricht, S. Van der Auwera, A. M. van Hemert, A. Viktorin, P. M. Visscher, Y. Wang, B. T. Webb, S. M. Weinsheimer, J. Wellmann, G. Willemsen, S. H. Witt, Y. Wu, H. S. Xi, J. Yang, F. Zhang, V. Arolt, B. T. Baune, K. Berger, D. I. Boomsma, S. Cichon, U. Dannlowski, E. J. C. de Geus, J. R. DePaulo, E. Domenici, K. Domschke, T. Esko, H. J. Grabe, S. P. Hamilton, C. Hayward, A. C. Heath, K. S. Kendler, S. Kloiber, G. Lewis, Q. S. Li, S. Lucae, P. A. F. Madden, P. K. Magnusson, N. G. Martin, A. M. McIntosh, A. Metspalu, B. Müller-Myhsok, M. M. Nöthen, M. C. O'Donovan, S. A. Paciga, N. L. Pedersen, B. W. J. H. Penninx, R. H. Perlis, D. J. Porteous, J. B. Potash, M. Preisig, M. Rietschel, C. Schaefer, T. G. Schulze, J. W. Smoller, H. Tiemeier, R. Uher, H. Völzke, M. M. Weissman, C. M. Lewis, D. F. Levinson, G. Breen, M. Agee, B. Alipanahi, A. Auton, R. K. Bell, K. Bryc, S. L. Elson, P. Fontanillas, N. A. Furlotte, B. S. Hromatka, K. E. Huber, A. Kleinman, N. K. Litterman, M. H. McIntyre, J. L. Mountain, E. S. Noblin, C. A. M. Northover, S. J. Pitts, J. F. Sathirapongsasuti, O. V. Sazonova, J. F. Shelton, S. Shringarpure, J. Y. Tung, V. Vacic, C. H. Wilson, K. Stefansson, D. H. Geschwind, M. Nordentoft, D. M. Hougaard, T. Werge, O. Mors, P. B. Mortensen, B. M. Neale, M. J. Daly, A. D. Børglum, Identification of common genetic risk variants for autism spectrum disorder. *Nat. Genet.* **51**, 431–444 (2019).

90. D. M. Howard, M. J. Adams, T. K. Clarke, J. D. Hafferty, J. Gibson, M. Shirali, J. R. I. Coleman, S. P. Hagenaars, J. Ward, E. M. Wigmore, C. Alloza, X. Shen, M. C. Barbu, E. Y. Xu, H. C. Whalley, R. E. Marioni, D. J. Porteous, G. Davies, I. J. Deary, G. Hemani, K. Berger, H. Teismann, R. Rawal, V. Arolt, B. T. Baune, U. Dannlowski, K. Domschke,

C. Tian, D. A. Hinds, M. Trzaskowski, E. M. Byrne, S. Ripke, D. J. Smith, P. F. Sullivan, N. R. Wray, G. Breen, C. M. Lewis, A. M. McIntosh, Genome-wide meta-analysis of depression identifies 102 independent variants and highlights the importance of the prefrontal brain regions. *Nat. Neurosci.* **22**, 343–352 (2019).

91. M. J. Gandal, P. Zhang, E. Hadjimichael, R. L. Walker, C. Chen, S. Liu, H. Won, H. van Bakel, M. Varghese, Y. Wang, A. W. Shieh, J. Haney, S. Parhami, J. Belmont, M. Kim, P. Moran Losada, Z. Khan, J. Mleczko, Y. Xia, R. Dai, D. Wang, Y. T. Yang, M. Xu, K. Fish, P. R. Hof, J. Warrell, D. Fitzgerald, K. White, A. E. Jaffe, PsychENCODE Consortium, M. A. Peters, M. Gerstein, C. Liu, L. M. Iakoucheva, D. Pinto, D. H. Geschwind, Transcriptome-wide isoform-level dysregulation in ASD, schizophrenia, and bipolar disorder. *Science*. **362**, eaat8127 (2018).

Acknowledgments:

We thank NIH NeuroBioBank, the University of Maryland School of Medicine Brain and Tissue Bank for providing post-mortem brain tissue samples. This work used the Vincent J. Proteomics/Mass Spectrometry Laboratory at UC Berkeley, supported in part by NIH S10 Instrumentation Grant S10RR025622. We thank Lori Kohlstaedt for her help in mass spectrometry data analysis. We thank Stephan Sanders, Roger Nicoll, Neelroop Parikshak, Tanzila Mukhtar, and Huda Zoghbi for comments on the manuscript.

Funding:

National Institute of Neurological Disorders and Stroke grant 5R35NS097305 (ARK)

National Institutes of Health S10 Instrumentation grant S10RR025622

National Human Genome Research Institute grant HG010898 (NS)

National Institute of Mental Health grant MH124619 (NS)

Author contributions:

Conceptualization: LW

Data curation: LW

Formal analysis: LW

Funding acquisition: ARK

Investigation: LW, LZ, ACS, SGG, SW, MW, BH, TL

Methodology: LW, KP, LZ, ACS, SGG, Jiani Li, PL, Jingjing Li, JMAG

Resources: SW, YP, EJH, EAW, MFP, RK, NS, AP

Software: LW, KP

Supervision: XP, JMAG, AAB, ZL, ARK

Visualization: LW, KP

Writing – original draft: LW

Writing – review & editing: KP, LZ, ACS, SGG, SW, MW, BH, Jiani Li, TL, YP, EJH, EAW, MFP, RK, NS, AP, PL, Jingjing Li, XP, JMAG, AAB, ZL, ARK

Competing interests: Authors declare that they have no competing interests.

Data and materials availability: All raw proteomic data will be deposited to ProteomeXchange through MassIVE. All processed data are available in the auxiliary supplementary tables and online at https://liwang.shinyapps.io/PSD_development_explorer/.

Supplementary Materials

Materials and Methods

Figs. S1 to S18

Tables S1 to S11

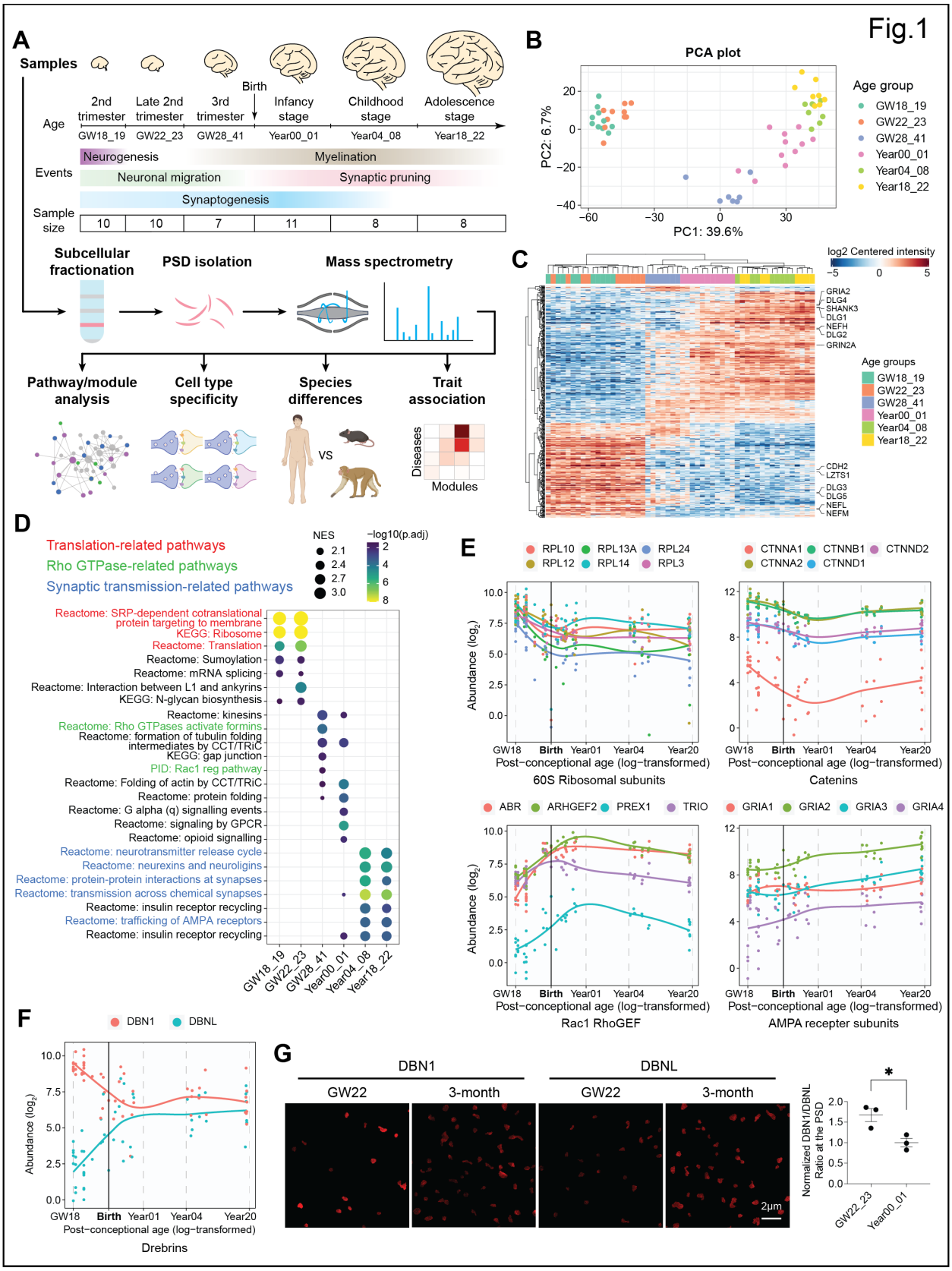
Fig.1
A
Samples
Birth
2nd trimester
Late 2nd trimester
3rd trimester
Infancy stage
Childhood stage
Adolescence stage
Age
GW18_19
GW22_23
GW28_41
Year00_01
Year04_08
Year18_22
Events
Neurogenesis
Myelination
Neuronal migration
Synaptic pruning
Synaptogenesis
Sample size
10
10
7
11
8
8
Subcellular fractionation
PSD isolation
Mass spectrometry
Pathway/module analysis
Cell type specificity
Species differences
Trait association
VS
Diseases
Modules
B
PCA plot
PC2: 6.7%
PC1: 39.6%
Age group
GW18_19
GW22_23
GW28_41
Year00_01
Year04_08
Year18_22
C
log2 Centered intensity
GRIA2
DLG4
SHANK3
DLG1
NEFH
DLG2
GRIN2A
CDH2
LZTS1
DLG3
DLG5
NEFL
NEFM
Age groups
GW18_19
GW22_23
GW28_41
Year00_01
Year04_08
Year18_22
D
Translation-related pathways
Rho GTPase-related pathways
Synaptic transmission-related pathways
NES
−log10(p.adj)
Reactome: SRP-dependent cotranslational protein targeting to membrane
KEGG: Ribosome
Reactome: Translation
Reactome: Sumoylation
Reactome: mRNA splicing
Reactome: Interaction between L1 and ankyrins
KEGG: N-glycan biosynthesis
Reactome: kinesins
Reactome: Rho GTPases activate formins
Reactome: formation of tubulin folding intermediates by CCT/TRiC
KEGG: gap junction
PID: Rac1 reg pathway
Reactome: Folding of actin by CCT/TRiC
Reactome: protein folding
Reactome: G alpha (q) signalling events
Reactome: signaling by GPCR
Reactome: opioid signalling
Reactome: neurotransmitter release cycle
Reactome: neurexins and neuroligins
Reactome: protein-protein interactions at synapses
Reactome: transmission across chemical synapses
Reactome: insulin receptor recycling
Reactome: trafficking of AMPA receptors
Reactome: insulin receptor recycling
E
RPL10
RPL13A
RPL24
RPL12
RPL14
RPL3
60S Ribosomal subunits
CTNNA1
CTNNB1
CTNND2
CTNNA2
CTNND1
Catenins
ABR
ARHGEF2
PREX1
TRIO
Rac1 RhoGEF
GRIA1
GRIA2
GRIA3
GRIA4
AMPA recepter subunits
Abundance (log2)
Post−conceptional age (log−transformed)
GW18
Birth
Year01
Year04
Year20
F
DBN1
DBNL
Drebrins
G
DBN1
DBNL
GW22
3-month
2μm
Normalized DBN1/DBNL Ratio at the PSD
GW22_23
Year00_01

Fig. 1. Changes in PSD composition during human neocortical development.

(A) Flow chart of the overall approach.

(B) PCA plots of the samples colored by their age groups.

(C) Hierarchical clustering of the samples based on proteins with differential abundance.

(D) Gene set enrichment analysis for individual age groups. NES: normalized enrichment score.

(E) Abundance patterns of representative PSD proteins.

(F) Abundance patterns of DBN1 and DBNL.

(G) Immunostaining of DBN1 and DBNL at DLG4 loci in the human neocortex (n = 3, 3 samples, scale bar: 2 μm). *$p < 0.05$; unpaired two-tailed *t* test.

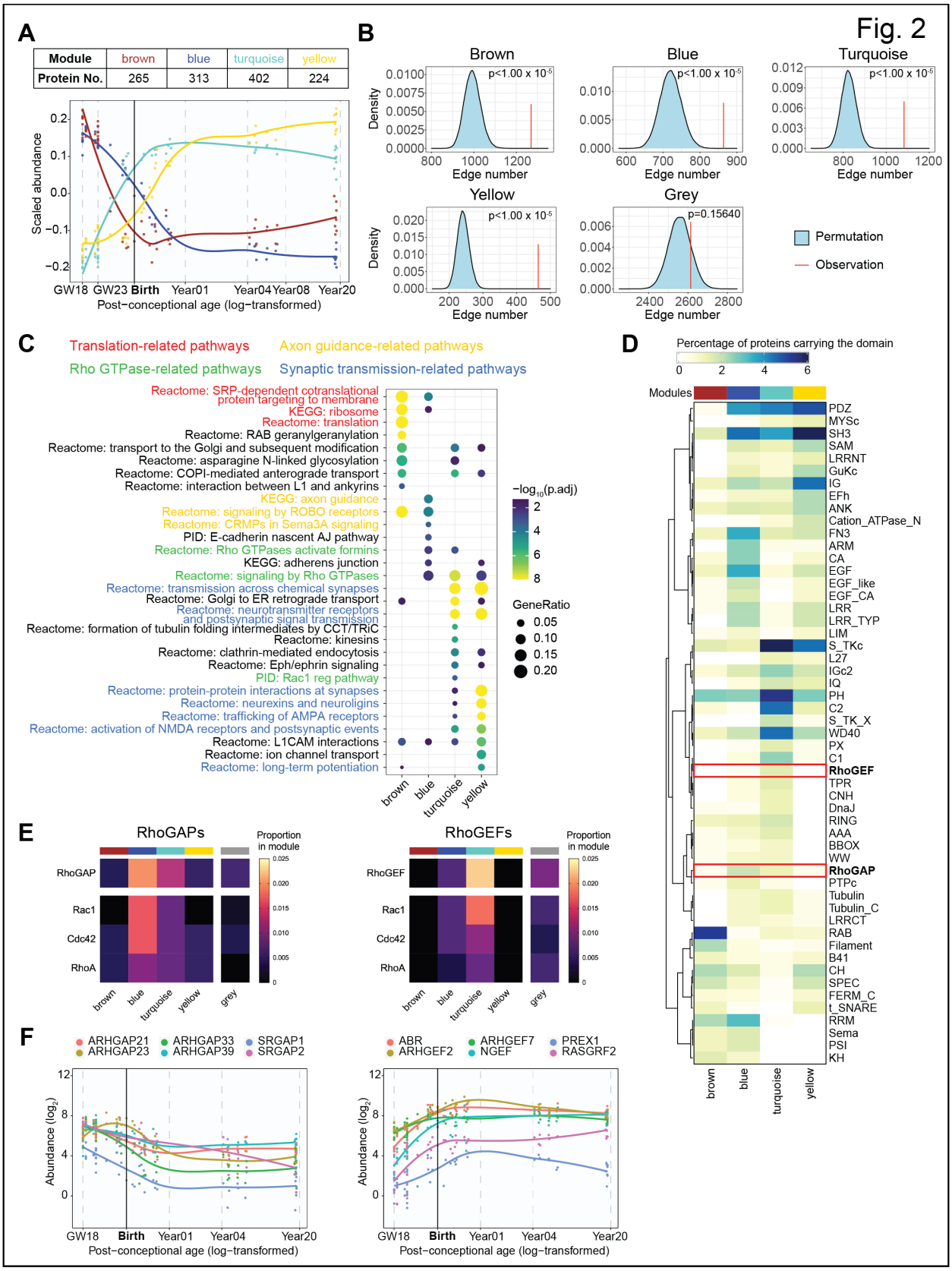
Fig. 2
A
Module | brown | blue | turquoise | yellow
Protein No. | 265 | 313 | 402 | 224
Scaled abundance
GW18 GW23 Birth Year01 Year04 Year08 Year20
Post−conceptional age (log−transformed)
B
Brown
Blue
Turquoise
Yellow
Grey
Density
Edge number
p<1.00 x 10-5
p=0.15640
Permutation
Observation
C
Translation-related pathways
Axon guidance-related pathways
Rho GTPase-related pathways
Synaptic transmission-related pathways
Reactome: SRP-dependent cotranslational protein targeting to membrane
KEGG: ribosome
Reactome: translation
Reactome: RAB geranylgeranylation
Reactome: transport to the Golgi and subsequent modification
Reactome: asparagine N-linked glycosylation
Reactome: COPI-mediated anterograde transport
Reactome: interaction between L1 and ankyrins
KEGG: axon guidance
Reactome: signaling by ROBO receptors
Reactome: CRMPs in Sema3A signaling
PID: E-cadherin nascent AJ pathway
Reactome: Rho GTPases activate formins
KEGG: adherens junction
Reactome: signaling by Rho GTPases
Reactome: transmission across chemical synapses
Reactome: Golgi to ER retrograde transport
Reactome: neurotransmitter receptors and postsynaptic signal transmission
Reactome: formation of tubulin folding intermediates by CCT/TRiC
Reactome: kinesins
Reactome: clathrin-mediated endocytosis
Reactome: Eph/ephrin signaling
PID: Rac1 reg pathway
Reactome: protein-protein interactions at synapses
Reactome: neurexins and neuroligins
Reactome: trafficking of AMPA receptors
Reactome: activation of NMDA receptors and postsynaptic events
Reactome: L1CAM interactions
Reactome: ion channel transport
Reactome: long-term potentiation
brown blue turquoise yellow
−log10(p.adj)
GeneRatio
D
Percentage of proteins carrying the domain
Modules
PDZ
MYSc
SH3
SAM
LRRNT
GuKc
IG
EFh
ANK
Cation_ATPase_N
FN3
ARM
CA
EGF
EGF_like
EGF_CA
LRR
LRR_TYP
LIM
S_TKc
L27
IGc2
IQ
PH
C2
S_TK_X
WD40
PX
C1
RhoGEF
TPR
CNH
DnaJ
RING
AAA
BBOX
WW
RhoGAP
PTPc
Tubulin
Tubulin_C
LRRCT
RAB
Filament
B41
CH
SPEC
FERM_C
t_SNARE
RRM
Sema
PSI
KH
E
RhoGAPs
RhoGEFs
Proportion in module
RhoGAP
RhoGEF
Rac1
Cdc42
RhoA
brown blue turquoise yellow grey
F
ARHGAP21 ARHGAP23 ARHGAP33 ARHGAP39 SRGAP1 SRGAP2
ABR ARHGEF2 ARHGEF7 NGEF PREX1 RASGRF2
Abundance (log2)
GW18 Birth Year01 Year04 Year20
Post−conceptional age (log−transformed)

Fig. 2. Protein modules of the developing human PSD with distinct functions.

(A) Scaled abundance patterns (module eigengene values) of four protein modules of the human PSD identified by WGCNA.

(B) Kernel density estimation of the null distributions of protein-protein interaction (PPI) numbers assuming no enrichment of PPI in individual modules; the vertical red lines indicate the observed PPI numbers in each module.

(C) Pathway enrichment analysis of each module (hypergeometric test).

(D) Distribution of protein domains in each module.

(E) Proportions of RhoGAPs and RhoGEFs and their subtypes in each module.

(F) Abundance patterns of RhoGAPs in the blue module and RhoGEFs in the turquoise module.

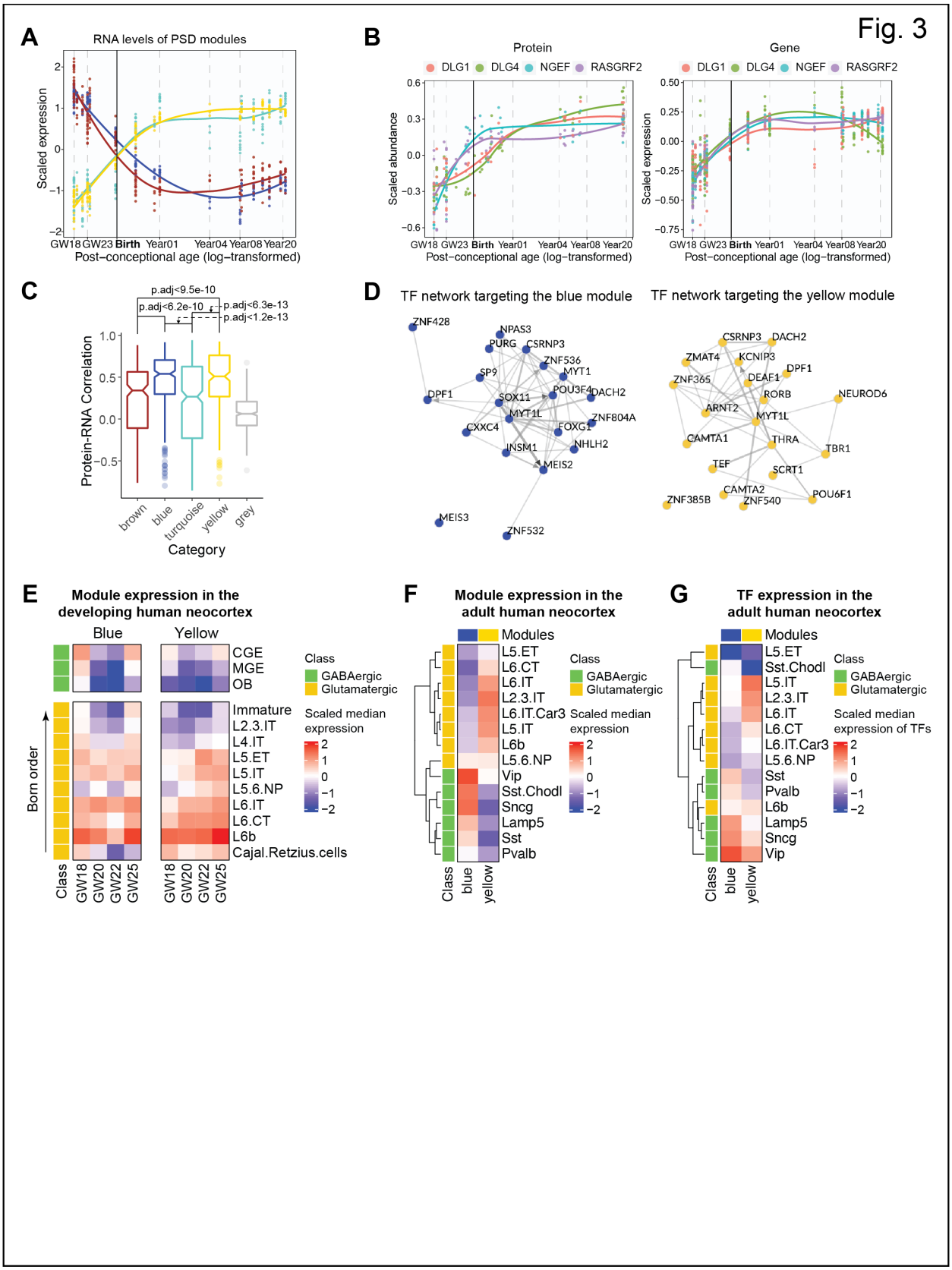
Fig. 3
A
RNA levels of PSD modules
Scaled expression
GW18 GW23 Birth Year01 Year04 Year08 Year20
Post−conceptional age (log−transformed)
B
Protein
Gene
DLG1 DLG4 NGEF RASGRF2
Scaled abundance
Scaled expression
C
p.adj<9.5e-10
p.adj<6.2e-10
p.adj<6.3e-13
p.adj<1.2e-13
Protein-RNA Correlation
brown blue turquoise yellow grey
Category
D
TF network targeting the blue module
TF network targeting the yellow module
ZNF428 NPAS3 PURG CSRNP3 ZNF536 MYT1 SP9 POU3F4 DACH2 DPF1 SOX11 MYT1L ZNF804A CXXC4 FOXG1 INSM1 NHLH2 MEIS2 MEIS3 ZNF532
CSRNP3 DACH2 ZMAT4 KCNIP3 DPF1 ZNF365 DEAF1 RORB NEUROD6 ARNT2 MYT1L CAMTA1 THRA TBR1 TEF SCRT1 CAMTA2 POU6F1 ZNF385B ZNF540
E
Module expression in the developing human neocortex
Blue
Yellow
CGE
MGE
OB
Immature
L2.3.IT
L4.IT
L5.ET
L5.IT
L5.6.NP
L6.IT
L6.CT
L6b
Cajal.Retzius.cells
Born order
Class
GW18 GW20 GW22 GW25
Class
GABAergic
Glutamatergic
Scaled median expression
F
Module expression in the adult human neocortex
Modules
L5.ET
L6.CT
L6.IT
L2.3.IT
L6.IT.Car3
L5.IT
L6b
L5.6.NP
Vip
Sst.Chodl
Sncg
Lamp5
Sst
Pvalb
Class
blue
yellow
G
TF expression in the adult human neocortex
Scaled median expression of TFs

Fig. 3. Transcription of PSD proteins and cell type specificity.

(A) Scaled median expression patterns of genes encoding proteins of the four PSD modules in the BrainSpan data.

(B) Scaled protein abundance and gene expression patterns of DLG1, DLG4, NGEF, and RASGRF2.

(C) Spearman correlation coefficients between protein abundance and gene expression of PSD proteins in each module.

(D) Transcription factor (TF) networks that regulate genes in the blue and yellow modules.

(E) Scaled median expression values of the blue and yellow modules in individual neuronal subtypes of the developing human neocortex.

(F) Scaled median expression values of the blue and yellow modules in individual neuronal subtypes of the adult human neocortex.

(G) Scaled median expression values of the TFs regulating the blue and yellow modules in individual neuronal subtypes of the adult human neocortex.

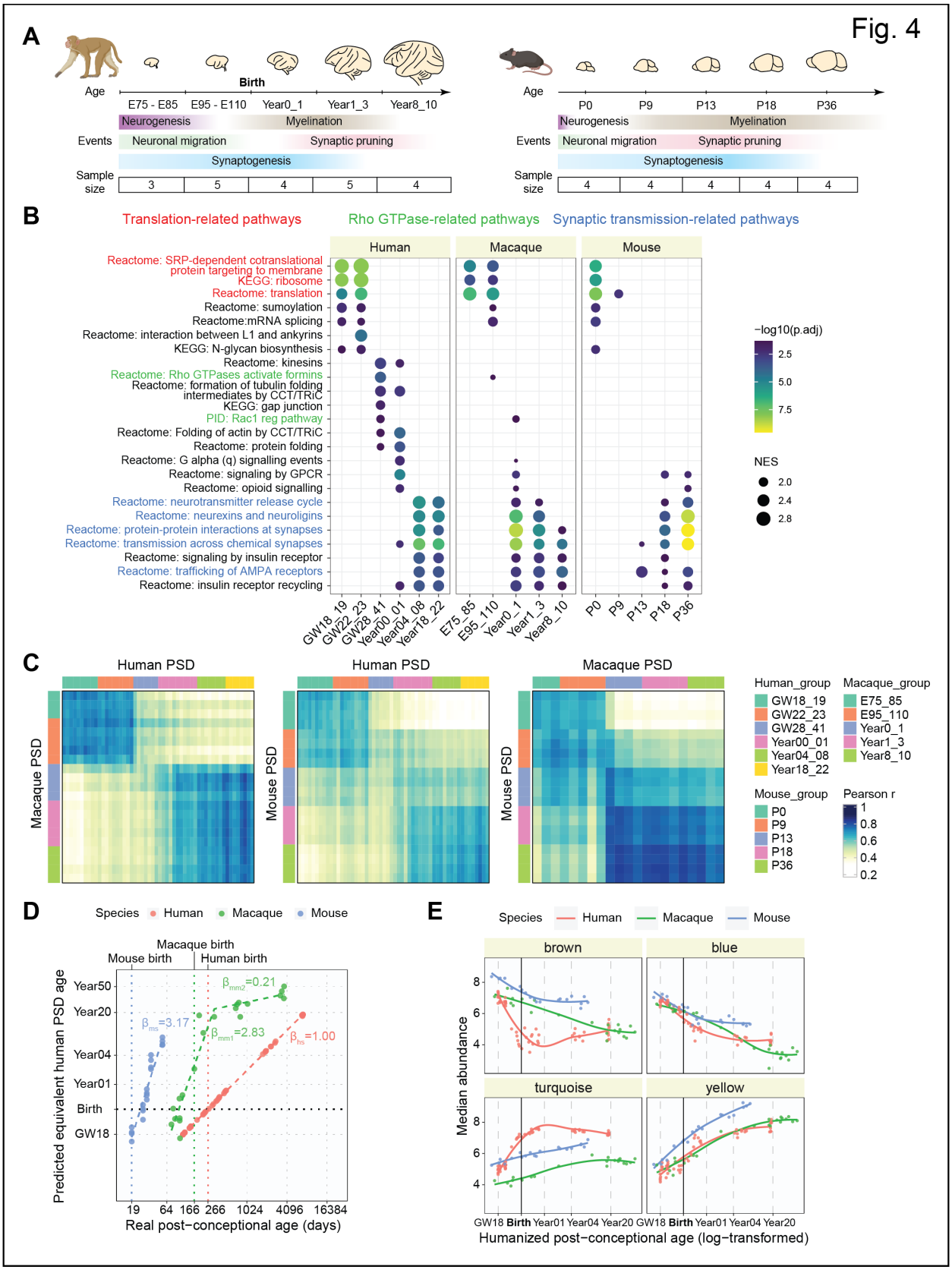
Fig. 4
A
Age
Birth
E75 - E85
E95 - E110
Year0_1
Year1_3
Year8_10
Neurogenesis
Myelination
Events
Neuronal migration
Synaptic pruning
Synaptogenesis
Sample size
3
5
4
5
4
P0
P9
P13
P18
P36
4
4
4
4
4
B
Translation-related pathways
Rho GTPase-related pathways
Synaptic transmission-related pathways
Human
Macaque
Mouse
Reactome: SRP-dependent cotranslational protein targeting to membrane
KEGG: ribosome
Reactome: translation
Reactome: sumoylation
Reactome:mRNA splicing
Reactome: interaction between L1 and ankyrins
KEGG: N-glycan biosynthesis
Reactome: kinesins
Reactome: Rho GTPases activate formins
Reactome: formation of tubulin folding intermediates by CCT/TRiC
KEGG: gap junction
PID: Rac1 reg pathway
Reactome: Folding of actin by CCT/TRiC
Reactome: protein folding
Reactome: G alpha (q) signalling events
Reactome: signaling by GPCR
Reactome: opioid signalling
Reactome: neurotransmitter release cycle
Reactome: neurexins and neuroligins
Reactome: protein-protein interactions at synapses
Reactome: transmission across chemical synapses
Reactome: signaling by insulin receptor
Reactome: trafficking of AMPA receptors
Reactome: insulin receptor recycling
GW18_19
GW22_23
GW28_41
Year00_01
Year04_08
Year18_22
E75_85
E95_110
Year0_1
Year1_3
Year8_10
P0
P9
P13
P18
P36
−log10(p.adj)
2.5
5.0
7.5
NES
2.0
2.4
2.8
C
Human PSD
Human PSD
Macaque PSD
Macaque PSD
Mouse PSD
Mouse PSD
Human_group
GW18_19
GW22_23
GW28_41
Year00_01
Year04_08
Year18_22
Macaque_group
E75_85
E95_110
Year0_1
Year1_3
Year8_10
Mouse_group
P0
P9
P13
P18
P36
Pearson r
1
0.8
0.6
0.4
0.2
D
Species
Human
Macaque
Mouse
Macaque birth
Mouse birth
Human birth
Predicted equivalent human PSD age
Year50
Year20
Year04
Year01
Birth
GW18
β_{ms}=3.17
β_{mm2}=0.21
β_{mm1}=2.83
β_{hs}=1.00
19
64
166
266
1024
4096
16384
Real post−conceptional age (days)
E
Species
Human
Macaque
Mouse
brown
blue
turquoise
yellow
Median abundance
8
6
4
GW18
Birth
Year01
Year04
Year20
Humanized post−conceptional age (log−transformed)

Fig. 4. Comparison of PSD development across humans, macaques, and mice.

(A) Schematic illustrating the developmental stages of macaque and mouse samples.

(B) Gene set enrichment analysis for individual age groups across species. NES: normalized enrichment score.

(C) Similarity matrices representing pairwise Pearson correlations between human, macaque, and mouse samples.

(D) Predicted equivalent human PSD ages. β indicates the coefficients of slope of the linear regression models in each species.

(E) Abundance patterns of the four PSD modules across species.

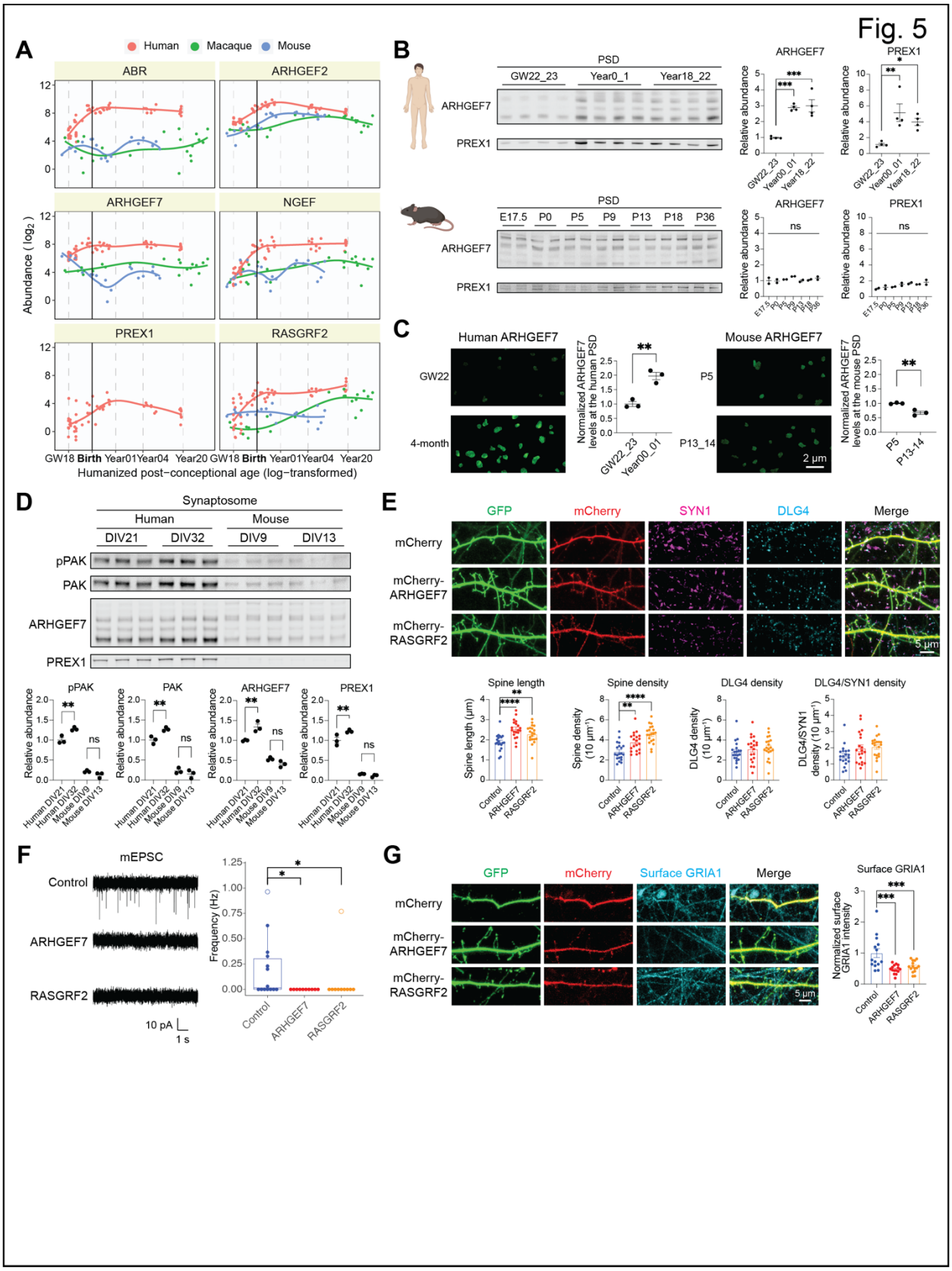
Fig. 5
A
Human
Macaque
Mouse
ABR
ARHGEF2
ARHGEF7
NGEF
PREX1
RASGRF2
Abundance (log2)
GW18 Birth Year01Year04 Year20
Humanized post−conceptional age (log−transformed)
B
PSD
GW22_23
Year0_1
Year18_22
ARHGEF7
PREX1
Relative abundance
E17.5 P0 P5 P9 P13 P18 P36
ns
C
Human ARHGEF7
Mouse ARHGEF7
GW22
4-month
P5
P13_14
2 μm
Normalized ARHGEF7 levels at the human PSD
Normalized ARHGEF7 levels at the mouse PSD
D
Synaptosome
Human
Mouse
DIV21
DIV32
DIV9
DIV13
pPAK
PAK
ARHGEF7
PREX1
Relative abundance
Human DIV21
Human DIV32
Mouse DIV9
Mouse DIV13
E
GFP
mCherry
SYN1
DLG4
Merge
mCherry-ARHGEF7
mCherry-RASGRF2
5 μm
Spine length
Spine density
DLG4 density
DLG4/SYN1 density
Control
ARHGEF7
RASGRF2
F
mEPSC
Control
ARHGEF7
RASGRF2
10 pA
1 s
Frequency (Hz)
G
GFP
mCherry
Surface GRIA1
Merge
mCherry-ARHGEF7
mCherry-RASGRF2
5 μm
Surface GRIA1
Normalized surface GRIA1 intensity

Fig. 5. Enhancement in RhoGEF proteins promotes neoteny of human synapses.

(A) Abundance patterns of RhoGEFs in the turquoise module across species.

(B) Immunoblots and quantification of representative RhoGEFs in the developing human (n = 4, 4, 4 samples) and mouse (n = 2, 2, 2, 2, 2, 2, 2 samples) PSD. *p < 0.05, **p < 0.01, ***p < 0.001; one-way ANOVA with Holm-Sidak's multiple comparisons test.

(C) Immunostaining of ARHGEF7 at DLG4 loci in the developing human and mouse neocortex (n = 3, 3, 3, 3 samples, scale bar: 2 μm). **p < 0.01; unpaired two-tailed *t* test.

(D) Immunoblots and quantification of representative RhoGEFs and downstream PAK signaling activity in the synaptosomes of culture primary human (n = 3, 3 samples) and mouse cortical neurons (n = 3, 3 samples). **p < 0.01; one-way ANOVA with Holm-Sidak's multiple comparisons test.

(E) Immunostaining of dendrites from primary human cortical neurons cultured six weeks *in vitro* transfected with mEGFP-C1 and vectors expressing mCherry, mCherry-ARHGEF7, or mCherry-RASGRF2 (n = 20, 20, 20 neurons, scale bar: 5 μm). **p < 0.01, ****p < 0.0001; one-way ANOVA with Holm-Sidak's multiple comparisons test.

(F) Miniature excitatory postsynaptic current (mEPSC) recording of primary human cortical neurons cultured six weeks *in vitro* transfected with mEGFP-C1 and vectors expressing mCherry, mCherry-ARHGEF7, or mCherry-RASGRF2 (n = 14, 10, 10 neurons). *p.adj < 0.05; Kruskal–Wallis test.

(G) Immunostaining against surface GRIA1 of dendrites from primary human cortical neurons cultured six weeks *in vitro* transfected with mEGFP-C1 and vectors expressing mCherry, mCherry-ARHGEF7, or mCherry-RASGRF2 (n = 14, 15, 15 neurons, scale bar: 5 μm). ***p < 0.001; one-way ANOVA with Holm-Sidak's multiple comparisons test.

Fig. 6

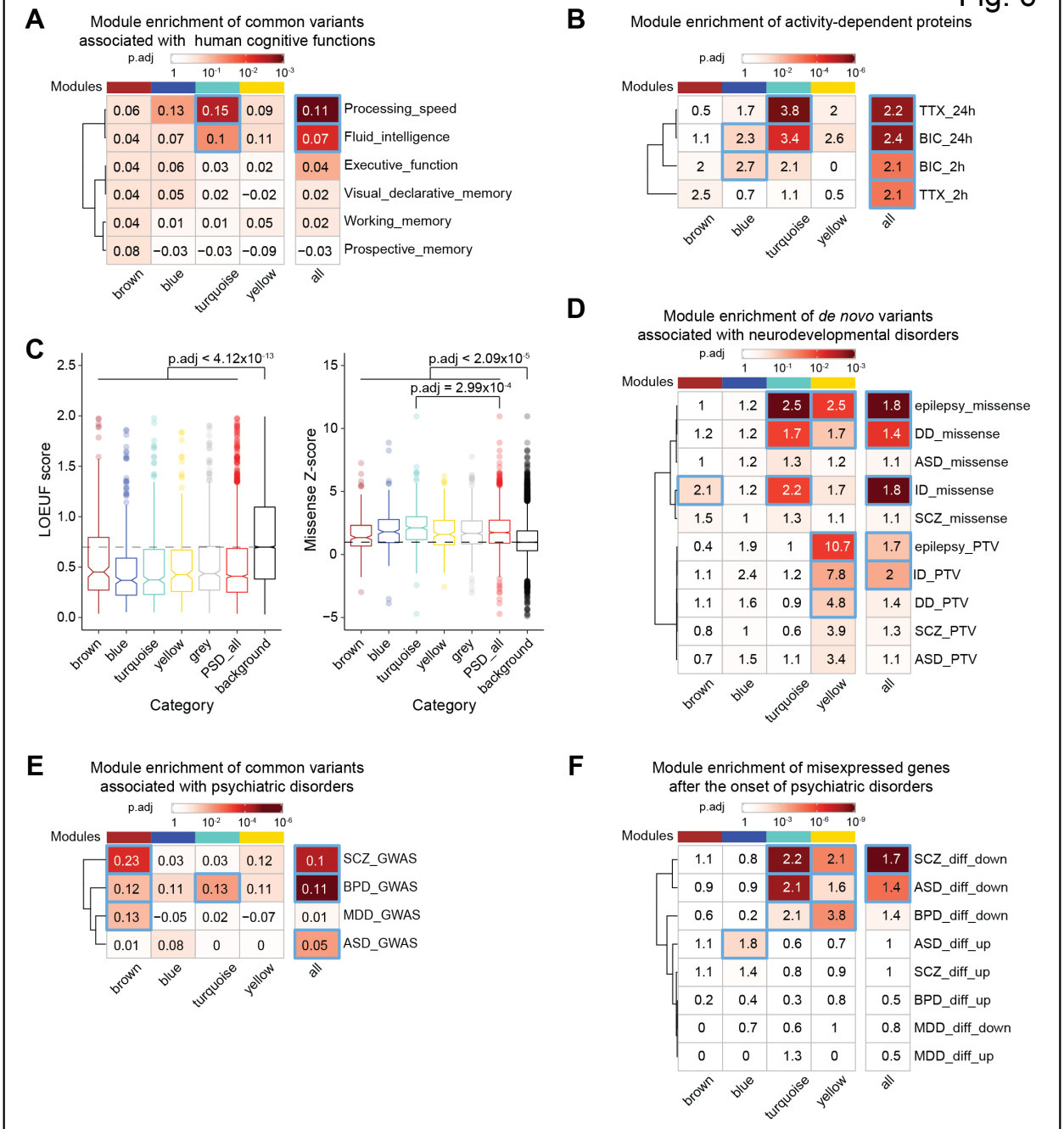
A
Module enrichment of common variants associated with human cognitive functions
p.adj
1 10-1 10-2 10-3
Modules
0.06 0.13 0.15 0.09 0.11 Processing_speed
0.04 0.07 0.1 0.11 0.07 Fluid_intelligence
0.04 0.06 0.03 0.02 0.04 Executive_function
0.04 0.05 0.02 −0.02 0.02 Visual_declarative_memory
0.04 0.01 0.01 0.05 0.02 Working_memory
0.08 −0.03 −0.03 −0.09 −0.03 Prospective_memory
brown blue turquoise yellow all
B
Module enrichment of activity-dependent proteins
p.adj
1 10-2 10-4 10-6
Modules
0.5 1.7 3.8 2 2.2 TTX_24h
1.1 2.3 3.4 2.6 2.4 BIC_24h
2 2.7 2.1 0 2.1 BIC_2h
2.5 0.7 1.1 0.5 2.1 TTX_2h
brown blue turquoise yellow all
C
p.adj < 4.12x10-13
LOEUF score
Category
brown blue turquoise yellow grey PSD_all background
p.adj < 2.09x10-5
p.adj = 2.99x10-4
Missense Z-score
Category
brown blue turquoise yellow grey PSD_all background
D
Module enrichment of de novo variants associated with neurodevelopmental disorders
p.adj
1 10-1 10-2 10-3
Modules
1 1.2 2.5 2.5 1.8 epilepsy_missense
1.2 1.2 1.7 1.7 1.4 DD_missense
1 1.2 1.3 1.2 1.1 ASD_missense
2.1 1.2 2.2 1.7 1.8 ID_missense
1.5 1 1.3 1.1 1.1 SCZ_missense
0.4 1.9 1 10.7 1.7 epilepsy_PTV
1.1 2.4 1.2 7.8 2 ID_PTV
1.1 1.6 0.9 4.8 1.4 DD_PTV
0.8 1 0.6 3.9 1.3 SCZ_PTV
0.7 1.5 1.1 3.4 1.1 ASD_PTV
brown blue turquoise yellow all
E
Module enrichment of common variants associated with psychiatric disorders
p.adj
1 10-2 10-4 10-6
Modules
0.23 0.03 0.03 0.12 0.1 SCZ_GWAS
0.12 0.11 0.13 0.11 0.11 BPD_GWAS
0.13 −0.05 0.02 −0.07 0.01 MDD_GWAS
0.01 0.08 0 0 0.05 ASD_GWAS
brown blue turquoise yellow all
F
Module enrichment of misexpressed genes after the onset of psychiatric disorders
p.adj
1 10-3 10-6 10-9
Modules
1.1 0.8 2.2 2.1 1.7 SCZ_diff_down
0.9 0.9 2.1 1.6 1.4 ASD_diff_down
0.6 0.2 2.1 3.8 1.4 BPD_diff_down
1.1 1.8 0.6 0.7 1 ASD_diff_up
1.1 1.4 0.8 0.9 1 SCZ_diff_up
0.2 0.4 0.3 0.8 0.5 BPD_diff_up
0 0.7 0.6 1 0.8 MDD_diff_down
0 0 1.3 0 0.5 MDD_diff_up
brown blue turquoise yellow all

Fig. 6. Association of human PSD modules with cognitive functions and brain disorders.

(A) Enrichment of common variants associated with human cognitive functions in PSD modules. The numbers indicate the MAGMA linear regression coefficient β. The blue borders denote p.adj < 0.05; MAGMA analysis on GWAS summary statistics.

(B) Enrichment of neuronal activity-dependent proteins in PSD modules. The numbers indicate the odds ratio. The blue borders denote p.adj < 0.05; hypergeometric test.

(C) Distribution of gnomAD LOEUF scores and missense Z-scores of genes in each category. Kruskal–Wallis test.

(D) Enrichment of de novo variants associated with neurodevelopmental disorders in PSD modules. The numbers indicate the odds ratio. The blue borders denote p.adj < 0.05; hypergeometric test.

(E) Enrichment of common variants associated with psychiatric disorders in PSD modules. The numbers indicate the MAGMA linear regression coefficient β. The blue borders denote p.adj < 0.05; MAGMA analysis on GWAS summary statistics.

(F) Enrichment of misexpressed genes after the onset of psychiatric disorders in PSD modules. The numbers indicate the odds ratio. The blue borders denote p.adj < 0.05; hypergeometric test.